NASA CONTRACTOR REPORT

NASA CR-998
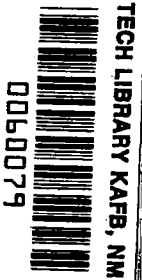
NASA CR-99

STUDIES OF PHOTOABSORPTION BY ATOMIC HYDROGEN, OXYGEN, AND NITROGEN

by R. B. Cairns and James A. R. Samson

STUDIES OF PHOTOABSORPTION BY ATOMIC

HYDROGEN, OXYGEN, AND NITROGEN

By R. B. Cairns and James A. R. Samson

Issued by Originator as Report No. GCA-TR-67-2-N

TABLE OF CONTENTS

STUDIES OF PHOTOABSORPTION BY ATOMIC HYDROGEN, OXYGEN, AND NITROGEN

By R. B. Cairns and James A. R. Samson

SUMMARY

This report contains an account of experiments made to study the photo-absorption properties of atomic hydrogen, oxygen, and nitrogen. The ultimate objective was the quantitative measurement of atomic photoionization cross sections. The results of the experiments have been combined with recent theoretical estimates of the cross sections and information from spectroscopic studies.

INTRODUCTION

In this report, experiments are described which were designed to yield information concerning specific values of the photoionization cross sections of atomic hydrogen $\sigma_{(H,\lambda)}$, oxygen $\sigma_{(O,\lambda)}$, and nitrogen $\sigma_{(N,\lambda)}$. The cross sections $\sigma_{(H,\lambda)}$ were measured first since they can be calculated exactly and, as a result, the validity and accuracy of the technique might be assessed.

The report is divided into the following sections:

BASIC EQUATIONS

The elementary equations which describe the absorption of radiation by a gas mixture composed of atoms and their parent diatomic molecules are presented in a suitable form.

EXPERIMENTAL TECHNIQUES

The techniques employed for dissociating H_2, O_2, and N_2 are described. The experimental procedures are discussed in sufficient detail to provide helpful information for further work in this field.

EXPERIMENTAL RESULTS

The results obtained for H, O, and N are described separately. This section also includes a brief account of related work which has been recently published.

CONCLUSION

The substance of this report is summarized and requirements for furthering the work discussed.

BASIC EQUATIONS

If radiation is absorbed by a gas consisting of ground state molecules and atoms only, the following equations can be used to evaluate their photo-ionization cross sections.

When monochromatic radiation of wavelength λ_1 is partially absorbed by the ground state molecular gas,

$$\ell n \ \frac{I_{(0,\lambda_1)}}{I_{(\lambda_1)}} = L \ \sigma_{(M,\lambda_1)} \ N_{(M)} \ , \qquad (1)$$

where   L is the length of the absorbing gas column (cm),

   $\sigma_{(M,\lambda_1)}$ is the total absorption cross section of the molecule (cm^2),

      $N_{(M)}$ is the number of molecules per cc, and

$I_{(0,\lambda_1)}/I_{(\lambda_1)}$ is the ratio of the intensity of radiation incident upon the gas to that transmitted.

If the molecular gas is partially dissociated, then

$$\ell n \ \frac{I_{(0,\lambda_1)}}{I'_{(\lambda_1)}} = L \left(\sigma_{(M,\lambda_1)} \ N'_{(M)} + \sigma_{(A,\lambda_1)} \ N'_{(A)} \right) , \qquad (2)$$

where $I'_{(\lambda_1)}$ is now the transmitted intensity,

   $\sigma_{(A,\lambda_1)}$ is the photoionization cross section of the atom, and

$N'_{(A)}$ and $N'_{(M)}$ are the number densities of the atoms and molecules, respectively.

If the mass of gas flowing through the system is unaltered when there is partial dissociation,

$$N_{(M)} = N'_{(M)} + 1/2 \; N'_{(A)} \tag{3}$$

Equations (1), (2), and (3) can be combined to give

$$\frac{1}{L} \ln \frac{I_{(\lambda_1)}}{I'_{(\lambda_1)}} = N'_{(A)} \left(\sigma_{(A,\lambda_1)} - \frac{1}{2} \sigma_{(M,\lambda_1)} \right) \tag{4}$$

At any wavelength λ_n, an equation corresponding to (4) applies which, when used in conjunction with Equation (4), gives

$$\sigma_{(A,\lambda_n)} = \frac{\ln I_{(\lambda_n)}/I'_{(\lambda_n)}}{\ln I_{(\lambda_1)}/I'_{(\lambda_1)}} \left(\sigma_{(A,\lambda_1)} - \frac{1}{2} \sigma_{(M,\lambda_1)} \right) + \frac{1}{2} \sigma_{(M,\lambda_n)} \tag{5}$$

Thus, the atomic cross section at any wavelength λ_n can be determined relative to that at wavelength λ_1 since all other parameters in Equation (5) can be measured. Equation (5) does not contain the product $N'_{(A)}L$ which is difficult to measure accurately since it requires a knowledge of the atom concentration at all points along the axis of the absorbing column (radial concentration gradients should also be known if the absorbed radiation is from a beam having an appreciable area of cross section).

If a wavelength $\lambda_{(p)}$ exists where $\sigma_{(A,\lambda_p)} = \frac{1}{2} \sigma_{(M,\lambda_p)}$, then from Equation (5)

$$\ln \frac{I_{(\lambda_p)}}{I'_{(\lambda_p)}} = 0 \; . \tag{6}$$

That is, the intensity of the transmitted radiation remains unaltered when partial dissociation occurs. The existence of such a condition would give a direct and absolute value of $\sigma_{(A,\lambda_p)}$, since $\sigma_{(M,\lambda_p)}$ can be measured using standard techniques. Thus, all relative measurements obtained using Equation (5) could be made absolute. It should be emphasized that, by this procedure, the absolute photoionization cross sections might be determined without any knowledge of either the number or spatial distribution of the absorbing atoms. However, should the method used for dissociating the molecular gas be effective in producing excited metastable atomic and/or molecular species, the analysis of the data is more complex. Such complications will be discussed as they arise.

EXPERIMENTAL TECHNIQUES

For measurements of the photoionization cross sections of atomic H, O, and N, it was necessary to dissociate the parent diatomic gases and to know the resulting partial gas pressures and gas temperatures. Consider the number N_A of atoms required per cm^3. If the length of the absorbing gas column were 20 cm (a length chosen such that no appreciable degree of recombination would occur along it), 20 percent of the incident radiation were absorbed, the atomic photoionization cross sections were greater than 10^{-18} but less than 10^{-17} cm^2 (see the theoretical cross sections presented later in this report), and the molecular absorption cross sections were negligible, then

$$\frac{\ln 1.25}{20 \times 10^{-18}} > N_A > \frac{\ln 1.25}{20 \times 10^{-17}} \tag{7}$$

or

$$1.1 \times 10^{16} > N_A > 1.1 \times 10^{15}$$

i.e., the fraction of molecules dissociated in a gas flow at 1 mm Hg pressure would be between 0.016 and 0.16.

There exists a variety of ways in which this degree of dissociation can be obtained:

(1)   thermally, at least for hydrogen at pressures less than about 1 mm Hg (see Figure 1),

(2)   in shock-induced plasmas,

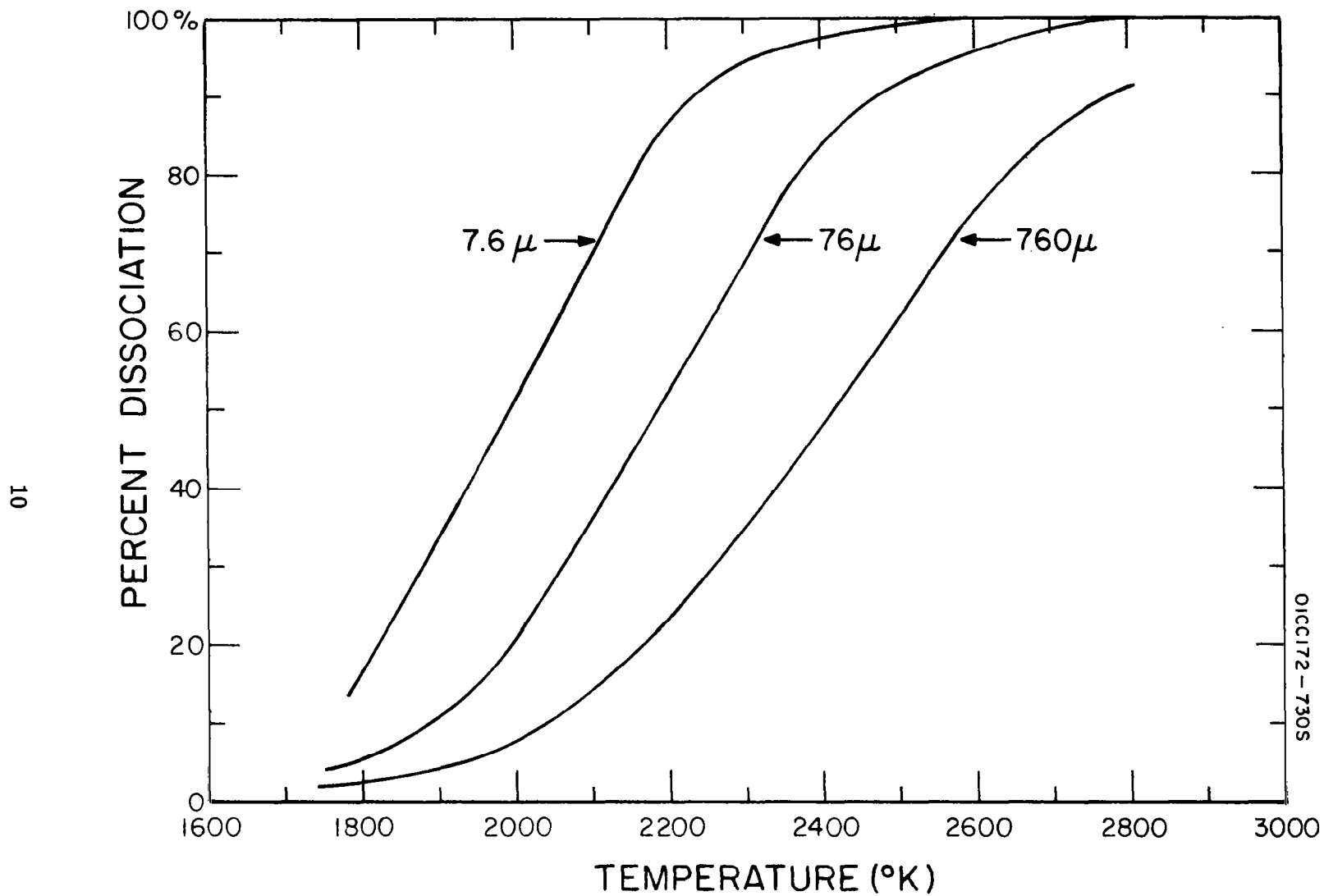(3)   in dc, rf, or microwave, pulsed or cw, electrode or electrodeless discharges,

Figure 1. The degree of dissociation of H_2 expressed as the ratio of the partial pressures of H to (H + H_2).

OICC172-730S

(4) in the afterglows of the above types of gas discharges.

The afterglow of a cw-electrodeless-rf or microwave discharge was selected since there are no large-scale transient fluctuations of temperature or atom concentration, the gas temperature is essentially room temperature, and there is no sputtering of electrode material resulting in increased atom losses by wall recombination. In an afterglow, the atom concentration is lower than in the discharge itself, but there are fewer unwanted excited atoms and molecules.

Dissociation of Hydrogen

Jennings and Linnett [1]* reported on the production of high concentrations of hydrogen atoms. At a gas pressure of 0.08 mm Hg, a 9.7 Mc/sec, 350 W rf discharge resulted in 50 to 60 percent of the gas being in the form of atoms at a distance of 25 cm from the discharge. At a pressure of 0.12 mm Hg, a Raytheon diathermy microwave unit produced a 10 percent atom concentration. Neynaber, et al. [2] reported that at 0.8 mm Hg, typically 45 percent of the gas emanating from their rf discharge was atomic. Bak and Rastrup-Andersen [3] using a Raytheon QK 62 magnetron to discharge H_2, reported that, at 25 cm from the discharge, 65 percent of the hydrogen was atomic. In the latter publication, the atom concentration was measured using a hot-wire detector, and it was assumed that the recombination of atoms on the wire surface was its sole heat source. There was thus a tacit assumption that neither excited atoms nor molecules existed in large quantities since these could deactivate on the wire surface. This same assumption appears in the work of Neynaber, et al. [2]. If this is

---

*Numbers in [ ] throughout text indicate reference numbers.

11

the case, the equations developed in the last section are applicable.

However, Lichten [4] reported the existence of a metastable excited state of H_2, $H_2c\ ^3\Pi_\mu$ (v=o) with a lifetime long enough to exist far downstream from the discharge. To excite this state, Lichten bombarded H_2 molecules with electrons of controlled energy, 11.9 eV. In any H_2 discharge, such metastables could be formed although their number density might be negligible.

The degree of dissociation of H_2 can be enhanced by the presence of small quantities of impurities; see, for example, the early work of Wood [5], Bichowsky and Copeland [6], and Lord Rayleigh [7]. Recently, an extensive study of the effect of gaseous impurities on the production of atomic hydrogen has been reported by Rony [8]. Contrary to expectation, Rony found that under his experimental conditions, water vapor had no effect on the yield of atomic hydrogen. He found, however, that the presence of water vapor in the gas flow produced an unexplained response from the Wrede Harteck gauge used to measure the atom concentration. Rony reported that the addition of O_2 increased the H atom yield from 9.2 percent with 7.1 percent O_2 to 16.4 percent with 15.8 percent O_2. Clearly the addition of contaminants in this quantity was undesirable for the cross section measurements. The relatively low degree of dissociation measured by Rony should also be noted.

Dissociation of Oxygen

Essentially, the same procedures can be followed as for hydrogen. The resulting degree of dissociation is, however, somewhat lower. In addition, a metastable species $O_2\ ^1\Delta_g$ has been detected in discharged O_2 [9].

Dissociation of Nitrogen

The evidence indicates that N_2 is more difficult to dissociate than either H_2 or O_2. Long-lived metastable species are also known to be produced in the dissociation process.

In summary, the simplest atomic gas for the present study appears to be hydrogen, where in a conventional rf or microwave discharge, a good supply of atoms can be expected free from metastable species, with the possible exception of H_2 $^c\Pi_\mu$.

Having produced the atoms, it was necessary to prevent them from recombining on the walls of the flow system and in the gas volume, and to have them flow at a speed and in a tube of diameter such that significant pressure gradients did not develop. The length of the open-ended absorption tube had also to be accurately defined. (No suitable end windows exist for use in the wavelength range 1000 to 500Å.)

The following estimate was made of the relative rate of atom loss due to wall and volume recombination.

Consider first, recombination on the walls. If γ is the fraction of surface collisions which leads to recombination, the loss rate per unit length of the tube is

$$\frac{1}{4} N_A \, \bar{v} \, 2\pi R \, \gamma \tag{8}$$

where N_A is the atom density, $\bar{v}$ the mean atomic speed and R the radius of the

tube. This atom loss, if assumed to be the only loss process, is equal to the difference between the atom flux into and that out of unit length of the tube, i.e.,

$$\bar{v}_f \, \pi R^2 \, \frac{dN_A}{dx} \tag{9}$$

where $\bar{v}_f$ is the average velocity of the gas stream and $\frac{dN_A}{dx}$ is the gradient of the atom density along the tube. Thus,

$$\left(\frac{dN_A}{dx}\right)_{wall} = - \frac{\bar{v} \, \gamma \, N_A}{2 \, \bar{v}_f \, R} \tag{10}$$

Therefore, to minimize wall losses, the coefficient γ should be small (this implies the maintenance of extremely clean pyrex walls) and the product $\bar{v}_f \, R$ should be large.

The atom decay in the volume of the gas is given by

$$\frac{dN_A}{dt} = \left(\frac{dN_A}{dx}\right)_{volume} \bar{v}_f = - k \, N_A^2 \, N_M \tag{11}$$

when k is the appropriate rate constant and N_M the number of molecules per cc. Therefore, to minimize volume losses, $\bar{v}_f$ should be large and care should be taken not to increase the rate constant k by impurity gases.

Consider the ratio of the two types of atom losses, namely

$$\frac{\left(\frac{dN_A}{dx}\right)_{wall}}{\left(\frac{dN_A}{dx}\right)_{volume}} = \frac{\bar{v} \, \gamma}{2R \, k \, N_A \, N_M} \, . \tag{12}$$

14

Typical values for the parameters in Equation (12) are: $R = 1$ cm, $\bar{v} = 2 \times 10^5$ cm/sec, $N_A = 5 \times 10^{15}$, $N_M = 3 \times 10^{16}$; and for hydrogen $\gamma = 10^{-4}$ for clean pyrex [10] and $k = 6.5 \times 10^{-32}$ cm^6/sec. Substituting these values into Equation (12) gives a ratio of the order of unity. That is, neither loss mechanism can be neglected relative to the other.

Having produced the atoms and pumped them without severe loss into the absorption cell, it was necessary to irradiate them at wavelengths shorter than 1000Å. The absorption cell assembly used for this purpose is shown diagramatically in Figure 2. Radiation was obtained from a high voltage condensed spark discharge. The gas in the light source was usually argon since its line spectrum is particularly dense and relatively intense in the required wavelength range. The radiation from the light source was dispersed in a 1/2-meter Seya monochromator. The wavelength resolution of this instrument was set for most experiments at 3Å. The radiation was then transmitted through the absorption cell and was detected using a photodetector (an aluminum plate detector, Figure 3, or a windowless photomultiplier). The background pressure in the entire system was about 5×10^{-5} mm Hg.

Tank gases (purity 99.5 percent) were used without further purification.
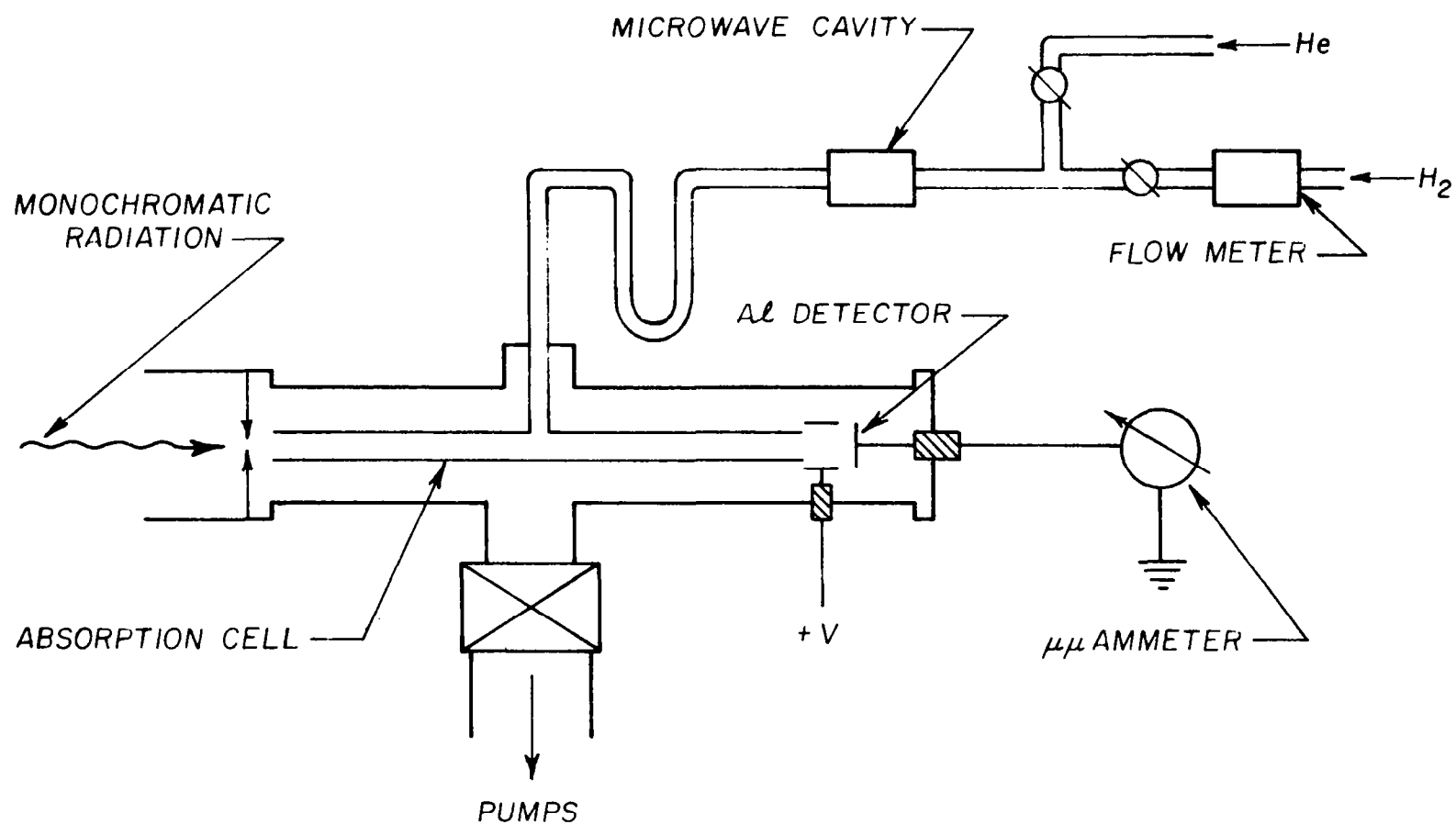
Figure 2. Absorption cell and gas flow system.

+V

ELECTRON COLLECTOR

TO $\mu\mu$ AMMETER

PHOTON
BEAM

ALUMINUM
PHOTOCATHODE
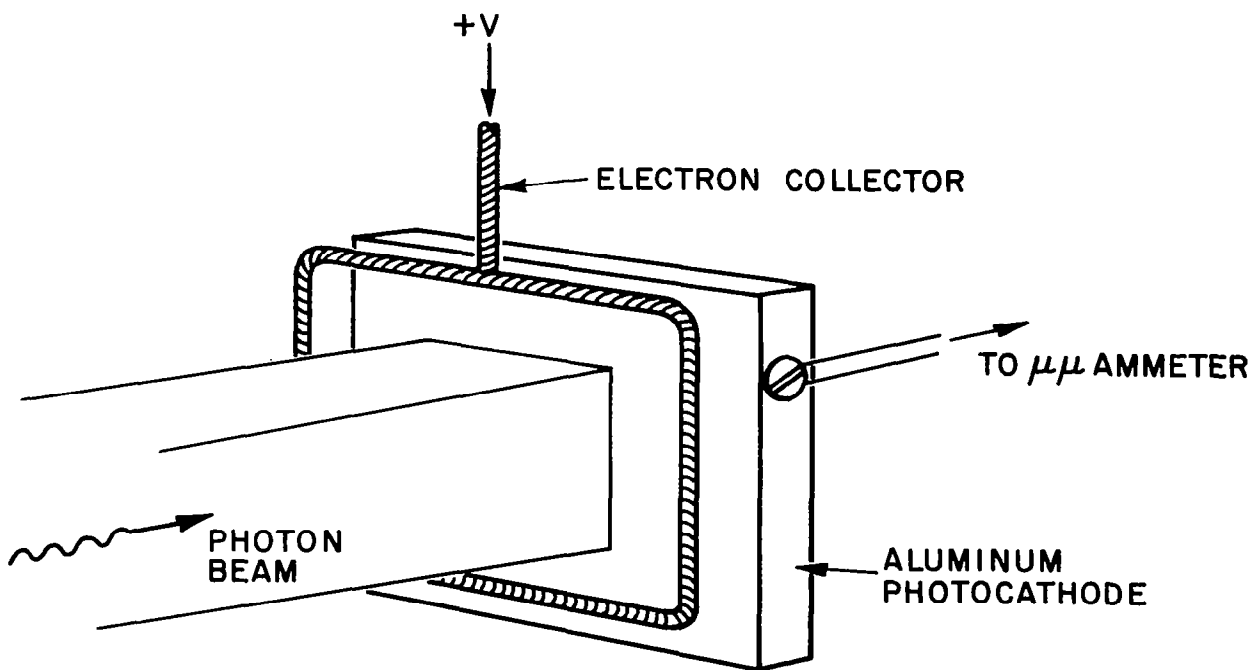
Figure 3. Aluminum photodetector.

EXPERIMENTAL RESULTS

Hydrogen

Measurements. — The energy level diagram of H_2 is given in Figure 4; see

Lichten [4]. Consider the electronic states. The state of lowest excitation

$b^3\Sigma_u^+$ is repulsive and dissociates in $\simeq 10^{-14}$ sec to form two 1S ground state

atoms. The dissociation energy is 4.48 eV. It is the existence of this $^3\Sigma_u^+$

state which accounts for the large degree of dissociation reported in H_2. The

$B^1\Sigma_u^+$ state decays via an allowed transition with a lifetime of about 6 x 10^{-10}

sec to the ground state $X^1\Sigma_g^+$. Thus, downstream from the discharge molecules

excited into this state will have decayed. The $a^3\Sigma_g^+$ state decays via an al-

lowed transition to the repulsive triplet state in 10^{-8} sec. As previously

mentioned, the $c^3\Pi_u$ state is metastable at least in its lowest vibrational

level (v=0) from which it can only decay via a forbidden magnetic dipole tran-

sition to the $b^3\Sigma_u^+$ state. The lifetime of such a transition is of the order

of 10^{-3} sec (which is sufficiently long for this species to exist far down-

stream from the discharge). Vibrational levels of the $c^3\Pi_u$ state higher than

(v=0) can decay to the $a^3\Pi_g^+$ state and are probably not metastable. All other

states of H_2 decay via allowed transitions to the ground state of H_2 or to the

repulsive states which result in dissociation. Atoms in the metastable 2S

state could be formed, but the energy required, $\simeq$ 15 eV, makes it probable

that the number of 2S atoms is small.

The number of molecules and atoms in excited electronic states in a hydro-

gen afterglow is, therefore, likely to be few. However, there is the question

of whether molecules are excited in large numbers into vibrationally excited

19
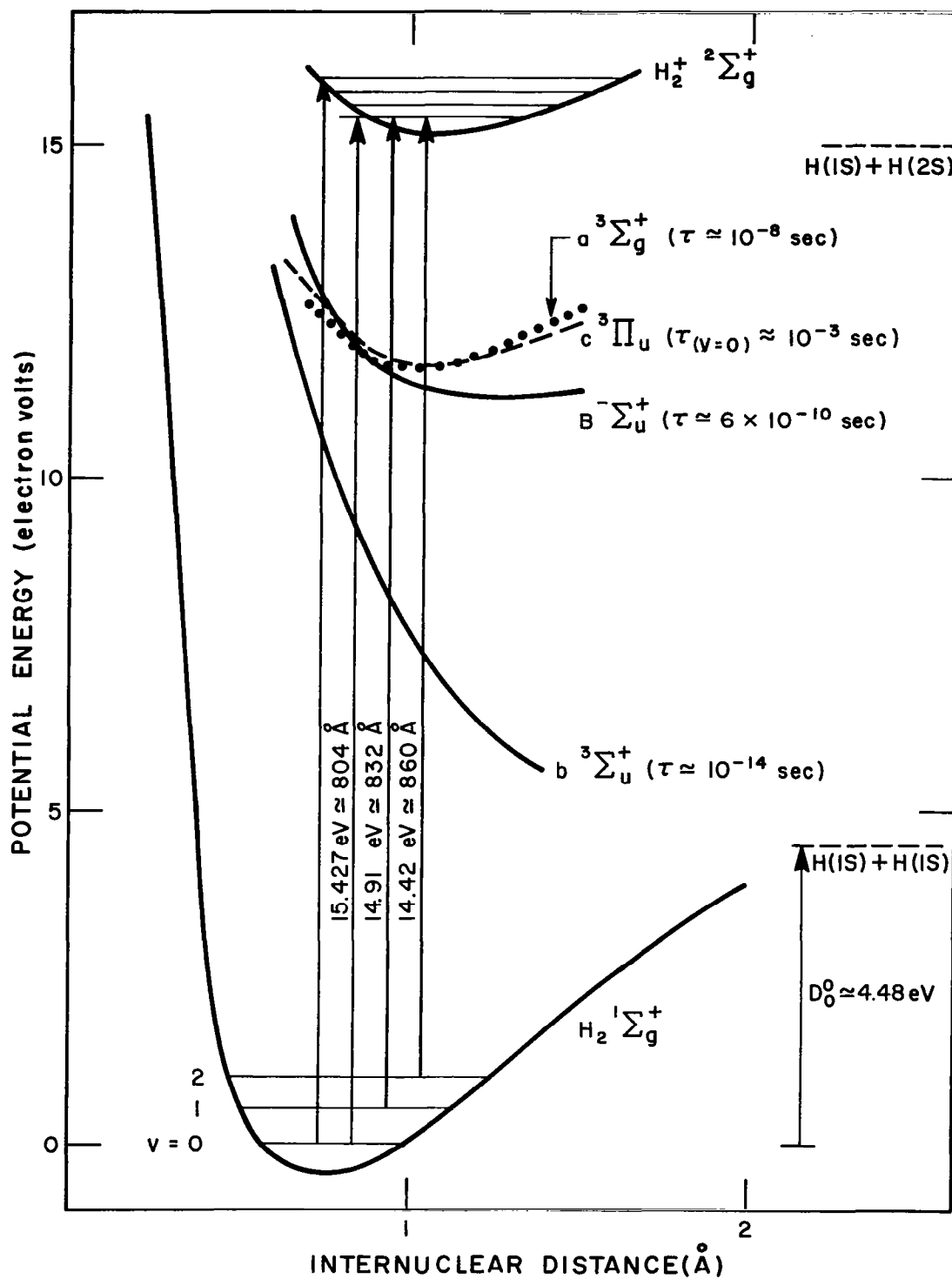
Figure 4. Potential energy curves for H_2.

levels of the ground electronic state. From the catalytic probe measurements mentioned earlier [3], this number was assumed to be small; however, no definitive information was available.

Hydrogen was introduced directly into the absorption cell through a flow meter and a needle valve. Hydrogen atoms were produced in an electrodeless microwave discharge maintained in a 0.1 cm i.d. Vycor tube using a Burdick Model MW-1, 100 W, 2450 Mc/sec diathermy unit, and an "Evenson" cavity manufactured by the Ophthos Instrument Company. This cavity has two tuning stubs for optimum matching to the discharge. The discharge was cooled nearly to room temperature by a flow of cold air. The products of the gas discharge passed through a U bend and a 78.5 cm long 1.5 i.d. Pyrex absorption cell before being pumped from the system. No provision was made for an absolute measurement of the hydrogen atom concentration, since it can be seen from Equation (5) that relative values of the cross section $\sigma_{(H)}$ could be obtained without this information. The relative values could then be placed on an absolute scale (see Equation (6)). The transmitted radiation was detected with the aluminum plate detector. This detector had sufficient sensitivity since its photoelectric yield was from 10 to 15 percent over the wavelength range considered. For a photon flux of approximately 10^8 photons/sec, this gave a photoelectric current of $\sim 10^7$ electrons/sec, i.e., a direct current of $\sim 10^{-12}$A. This current was measured with a Keithley Model 417 picoammeter.

Measurements were made of the intensity of the radiation incident $(I_{(o\lambda)})$ and of that transmitted through both neutral $(I_{(\lambda)})$ and discharged $(I'_{(\lambda)})$ H_2 at wavelengths in the spectral region 912Å (the ionization threshold of H) to 804Å. At wavelengths shorter than 804Å, ground state, H_2 $^1\Sigma_g^+$ (v=0) ionized

and had a sufficiently large photoionization cross section that both $I_{(\lambda)}$ and $I'_{(\lambda)}$ were too small to be measured accurately.

A typical set of data is presented in Figures 5(a) and (b). In Figure 5(a), the intensity $I_{(o\lambda)}$ of the unabsorbed radiation is plotted as a function of wavelength (background current from the detector arising from stray light was negligible). The fact that the sensitivity of the photodetector was wavelength dependent was of no concern in this experiment, since intensity ratios only were required. In Figure 5(b) are shown the intensities $I_{(\lambda)}$ and $I'_{(\lambda)}$. The following facts can be directly inferred from this figure. Hydrogen atoms in the ground $1^2S_{1/2}$ state were formed in the discharge as is shown by the absorption threshold at 912Å. At all wavelengths between 912 and 825Å, $I_{(\lambda)}$ was greater than $I'_{(\lambda)}$, i.e., if the data are interpreted according to Equation (5) $\sigma_{(H,\lambda)} > 1/2 \; \sigma_{(H_2,\lambda)}$ as would be expected from the theoretical values of $\sigma_{(H,\lambda)}$ and the experimental values of $1/2 \; \sigma_{(H_2,\lambda)}$. However, when H_2 was discharged, there was a nearly constant background current from the detector. The current was unaltered when the photon beam from the monochromator was switched off, and, therefore, it originated either from products formed within the microwave discharge or scattered radiation from the discharge. To determine whether scattered light was the cause, the following test was made. A liquid N_2 filled dewar was placed over the U bend in the flow tube between the discharge and the absorption cell. This resulted in an almost total reduction of the background current. This procedure could not have reduced the intensity of scattered radiation reaching the detector. It was, therefore, concluded that excited molecules or atoms formed within the discharge were deactivated with increased probability on the cold Pyrex surface. A further cause of the background
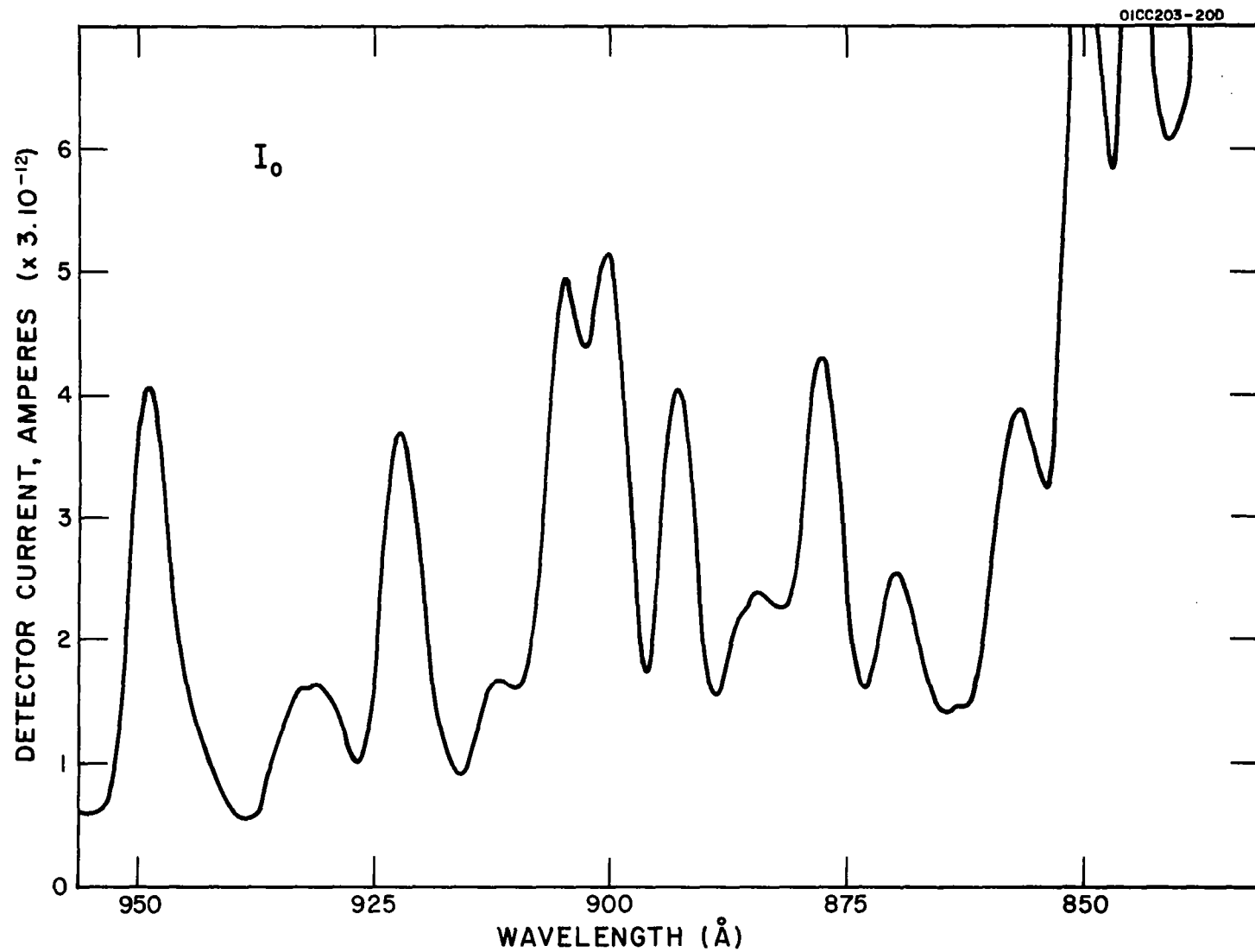
Figure 5(a). The relative intensity I_o of radiation incident upon
the absorbing gas as a function of wavelength.
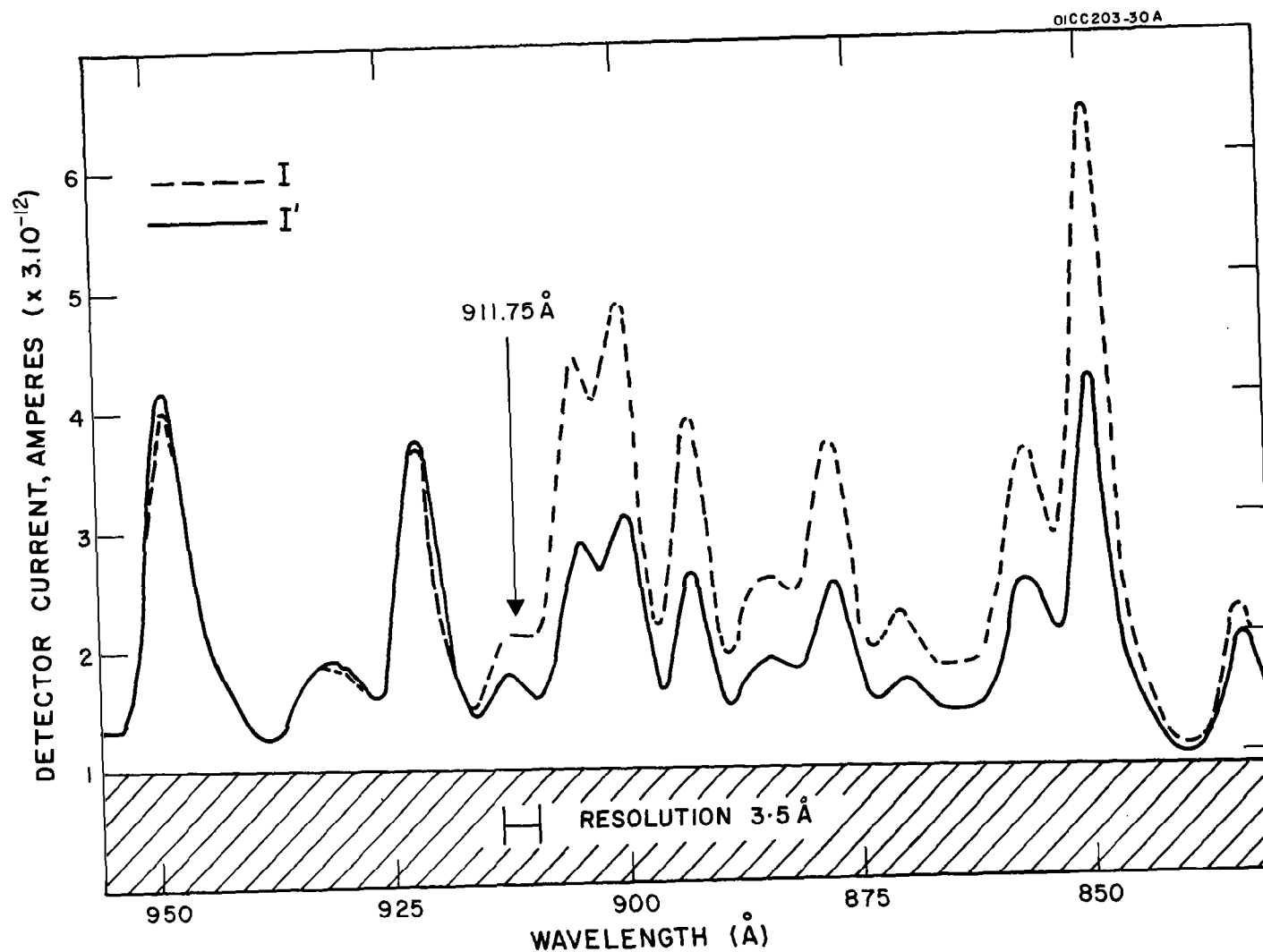
Figure 5(b). The relative intensities I and I' of the radiation transmitted through H_2 and discharged H_2, respectively. The background current, which was zero for the curve I, has been nomalized to that obtained with the curve I'.

24

current could have been atoms recombining on the surface of the detector, since the energy released per recombination (4.5 eV) is nearly equal to the work function of aluminum. This possible mechanism could not be simply discarded, since any procedure which totally removed the background current also removed the atoms. However, the number density of H atoms could be altered by changing the power dissipated in the microwave discharge without a corresponding change in the background current.

If the species causing this current were H_2 $c^3\Pi_u$ molecules and/or H $2^2S_{1/2}$ atoms, it was necessary to know their combined number density (M). The number M was estimated from the equation

$$M = \frac{ci}{\bar{\eta}\ \bar{v}_f\ e\ \pi\ R^2}\ ,$$ (13)

where   i is the background current ($\simeq 3 \times 10^{-12}$A, see Figure 5(b)),

e is the electronic charge,

c is a geometrical factor which was approximately equal to 5,

$\bar{\eta}$ is an average efficiency of ejection, and

$\bar{v}_f$ and R have been previously defined.

A reasonable value of $\bar{v}_f$ gives $M \simeq 10^4/\bar{\eta}$. Should the efficiency for electron ejection $\bar{\eta}$ be as low as 10^{-4}, M would be 10^8 and would represent a concentration of only about 1 part in 10^8 in the flowing gas. The species H_2 $c^3\Pi_u$ and H $2^2S_{1/2}$ were, therefore, not considered to be a significant source of error. Further evidence that these species existed in small quantity was obtained from the fact that there was no measurable increase in absorption when the discharge was switched on at wavelengths longer than 912Å at

which both of these species would photoionize.

These species were ignored, and the data obtained were interpreted according to Equation (5) to give relative values of $\sigma_{(H,\lambda)}$. These values were normalized to that given by Beynon and Cairns [11] at 850Å and are presented in Figure 6. There was fair agreement with the theoretical cross sections down to 850Å. At shorter wavelengths, there was a large discrepancy. Both the apparent agreement at wavelengths longer than 850Å, and an analysis of the probable experimental error suggests that the large differences between the experimental and theoretical values below 850Å must be caused by a systematic experimental error. Such an error could only be ascribed to the presence of further excited species in the discharged gas. That is, species in larger quantities than those causing electron emission from the photodetector. Their energies of excitation were, therefore, probably less than the work function of aluminum. Reference to the potential energy curves of H_2 (Figure 4) indicates that such species could be vibrationally or rotationally excited states of the ground state H_2 $^1\Sigma_g^+$. The thresholds for ionization from the v=1 and v=2 levels of H_2 $^1\Sigma_g^+$ occur at 832 and 860Å, respectively. If vibrationally excited molecules existed in appreciable quantities, systematic errors due to their neglect would certainly be apparent at wavelengths shorter than their ionization thresholds. A technique for confirming whether H_2 $^1\Sigma_g^+$ molecules did exist in the excited vibrational levels v=1 or 2 was devised. Measurements were made of the number of ion pairs produced in the absorption cell when the discharged gas was irradiated at wavelengths shorter than 860Å. For this purpose, the absorption cell was converted into an ionization chamber by placing within it two fine nickel wires. One of the wires was held at a positive potential and the other,
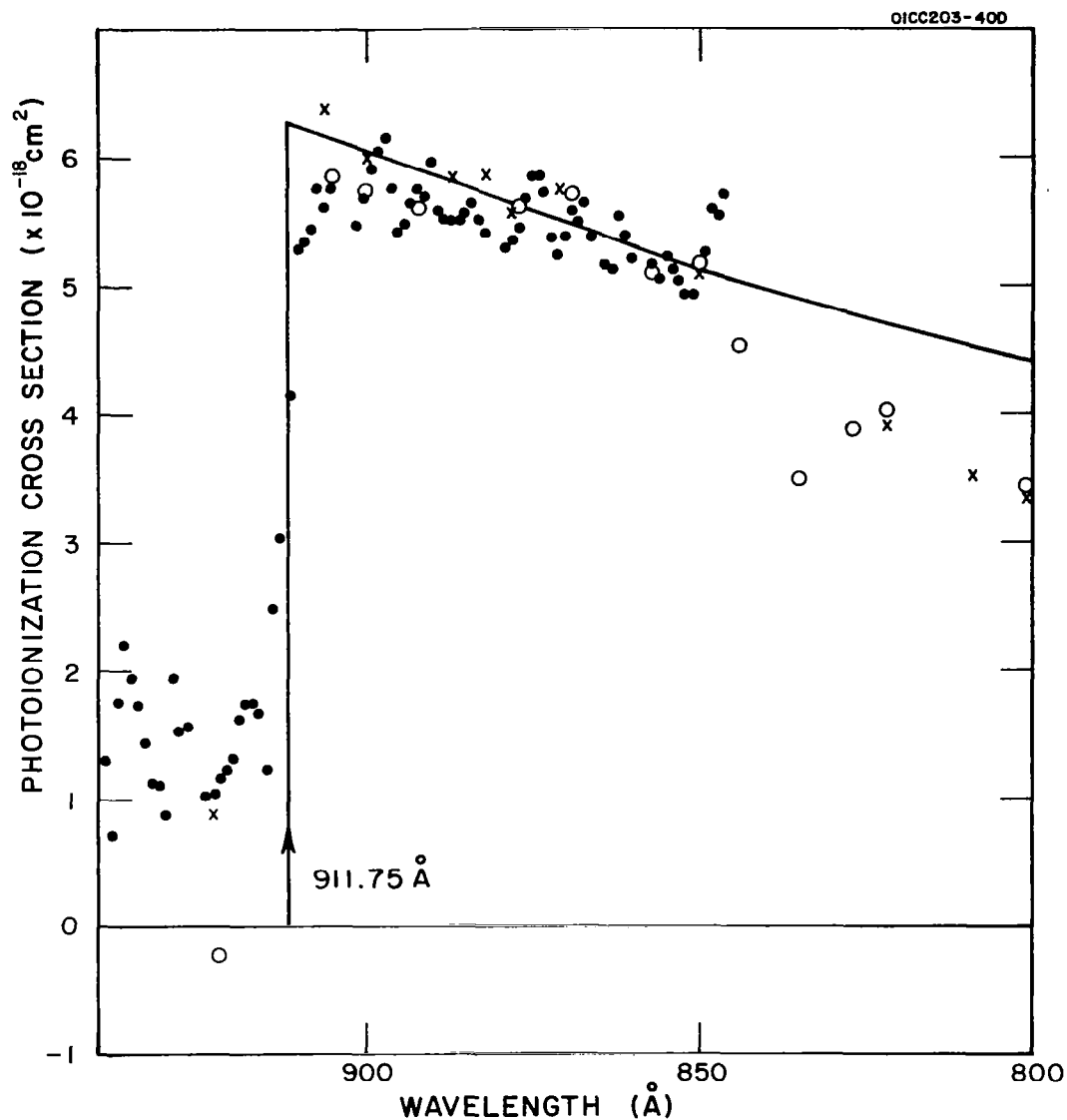
Figure 6. The photionization cross section of atomic hydrogen calculated using Equation (5). The symbols O, X and 0 denote three sets of data, the first two of which were obtained with H_2 alone flowing into the system. The third set (0) was calculated from data obtained with a H_2 - He mixture flowing into the system. The percentage experimental error at wavelengths longer than the ionization threshold, 912Å, was large since, in this region, there was little change in absorption when the gas was discharged. The solid line represents the theoretical cross section.

the positive ion collector, was attached to a picoammeter. The results obtained are shown in Figure 7. With H_2 only in the absorption cell, large ionization currents were obtained at wavelengths shorter than 804Å due to the direct photoionization of H_2 $^1\Sigma_g^+$. At longer wavelengths, photoelectric emission from the wires and the ionization of small quantities of gaseous impurities caused the background current shown as a broken line in Figure 7. With discharged H_2 in the ionization chamber, there was an increase (Δi) in the ion current at wavelengths shorter than 912Å. Evaluation of the ratios $\Delta i/I_{o(\lambda)}$ showed that the large increase in ion current at wavelengths shorter than 840Å could not be attributed to the direct photoionization of $H(1\ ^2S_{1/2})$ atoms. It could most probably be accounted for by the presence of H_2 in the first vibrational and in rotational levels of the ground electronic state.

No technique could be found which would remove these excited molecules, without causing atom recombination or inhibiting the production of atoms. As a result, these species produced a systematic error in the determination of $\sigma_{(H,\lambda)}$. This error was not confined to any limited wavelength region, but the evidence suggests that it was not large in the range 912 to 840Å.

Discussion of Results. — The results obtained are discussed in the following sections: (a) gaseous products from discharged hydrogen and (b) the photo-absorption of these products.

(a) Molecular hydrogen when discharged at microwave frequencies in an electrodeless system is partially dissociated. The afterglow of the discharge contains both ground state hydrogen molecules and atoms. The molecules were identified from their characteristic absorption properties and photoionization
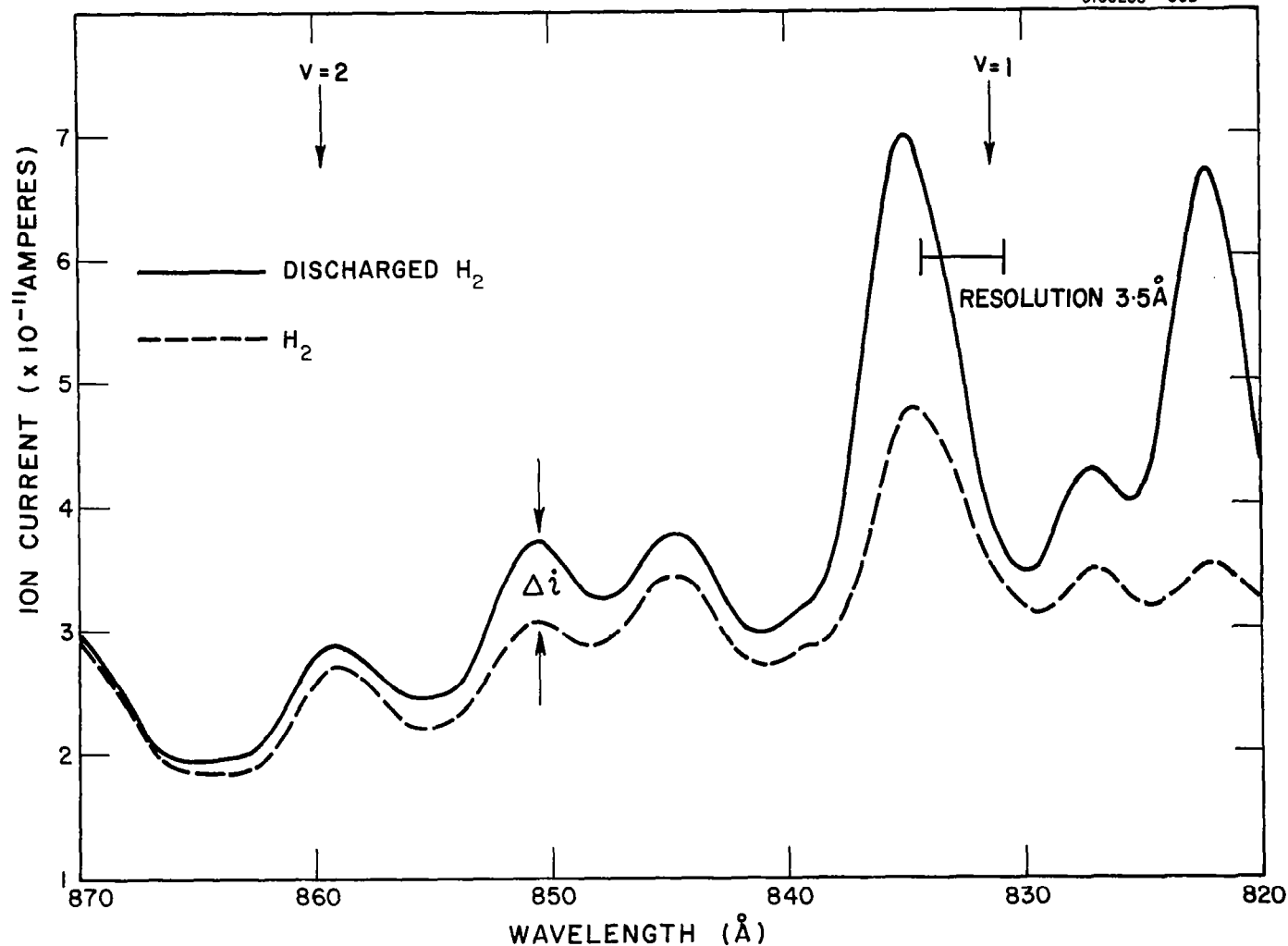
Figure 7. Photionization currents measured using the ionization chamber. The difference between the ordinates of the two curves (Δi) represents the increase in photoionization current when H_2 was discharged. The arrows labeled v = 1 and v = 2 indicate, respectively, the wavelengths shorter than which H_2 in the first and second vibrational levels of its ground state can be ionized.

threshold at 804Å. The atoms were identified from their photoionization thresh-old at 912Å. The average atom concentration within the absorption cell, i.e., at distances between 25 and 100 cm from the discharge, was about 1.3×10^{15} cm^3. (This estimate was made using the data obtained in the wavelength region 912 to 840Å, where systematic errors appeared to be small.) This meant that about 7 percent of the absorbing gas was in the form of ground state atoms. If the tank gas flowing to the discharge was dried by passage through a liquid nitro-gen cooled trap, the atom concentration was reduced. The use of absorption techniques to measure the relative atom concentrations is less ambiguous than the use of differential manometers (see Rony [8]) or thermocouples (see Bak, et al. [3]). Species with energies of excitation greater than the work func-tion of aluminum were produced in small numbers. These could be H_2 $c^3\Pi_u$ (v=0) molecules or H(2S) atoms or could possibly be owing to trace impurities in the tank gas, e.g., H_2O. In addition, molecular hydrogen was produced in states of lower excitation. These states could not be positively identified but the photoionization data suggest that they were predominantly H_2 $^1\Sigma_g^+$ molecules in the first vibrational and associated rotational levels.

(b) In the wavelength region 912 to 850Å, the absorption cross section of atomic hydrogen calculated on the assumption of there being only ground state atoms and molecules present is in fair agreement with the theoretical values, i.e., the systematic error owing to the neglect of excited species was small. This error would result in a difference between the theoretical and experimental values of the atomic hydrogen (photoabsorption) cross section given by:

$$\sigma_{(H,\lambda)\text{theory}} - \sigma_{(H,\lambda)\text{exp.}} = \frac{1}{N'_{(H)}} \sum_{\ell=1}^{n} N^{\ell}_{(H_2^*)} \left(\sigma_{(H_2,\lambda)} - \sigma^{\ell}_{(H_2^*,\lambda)} \right) , \quad (14)$$

where there are n different excited species.

It can be seen from this expression that $\sigma_{(H,\lambda)\text{theory}} \simeq \sigma_{(H,\lambda)\text{exp.}}$ if either

$$N'_{(H)} \gg \sum_{\ell=1}^{n} N^{\ell}_{(H_2^*)} \quad (15)$$

or

$$\sigma_{(H_2,\lambda)} \simeq \sigma^{\ell}_{(H_2^*,\lambda)} \quad (16)$$

Since $N'_{(H)}$ remained constant while data were obtained in both the wavelength regions 912 to 850Å and 850 to 804Å, it was concluded that the relatively small systematic errors in the 912 to 850Å region resulted from the condition $\sigma_{(H_2,\lambda)} \simeq \sigma^{\ell}_{(H_2^*,\lambda)}$.

The data presented show that quantitative absorption spectroscopy in the wavelength range 912 to 850Å can provide an estimate of the average number density of hydrogen atoms in a flowing H_2 afterglow with an accuracy of about ± 15 percent. Measurements made in hydrogen afterglows which have not taken account of metastable molecules should be reviewed in the light of these findings.

The Atomic Hydrogen Cross Section at Wavelengths Shorter Than 500Å

The theoretical formula for the photoionization cross sections of atomic hydrogen is essentially exact at wavelengths shorter than 500Å as well as in the wavelength range so far discussed. Some comments on and references to the theoretical work are given below. Exact calculations on hydrogen like systems have been made by Suguira [12], Gaunt [13], and Menzel and Pekeris [14]. The cross section is given by

$$\sigma = g(32 \, \pi^2 \, e^6 \, R)/(3^{3/2} \, h^3 \, \nu^3 \, n^5) \tag{17}$$

that is

$$\sigma(Mb) = 1.044 \times 10^{-8} \, g\lambda^3 \, (\text{Å}) \, ,$$

where R is the Rydberg constant, n is the principal quantum number, and g is the Gaunt factor which is a function of the frequency ν. If we set g = 1 in Equation (17), $\sigma(H)$ reduces to that given by Kramers [15]. The Gaunt factors vary from 0.8 at threshold to a maximum of 1.0 at approximately 200Å, then fall rapidly to extremely low values in the X-ray region. Using the Gaunt factors tabulated by Karzas and Latter [16] and Equation (17), the theoretical photoionization cross sections for atomic hydrogen have been obtained and are shown in Figure 8 as a function of wavelength. The values are tabulated in Table 1. The cross sections for molecular hydrogen have been measured between 200 and 450Å [17]. These values, divided by two, are also shown in Figure 8. On average, they are about a factor of two greater than the theoretical values. This disagreement is not surprising since there are no inner shell electrons in hydrogen and the two electrons are involved in the molecular bond. At 44Å,
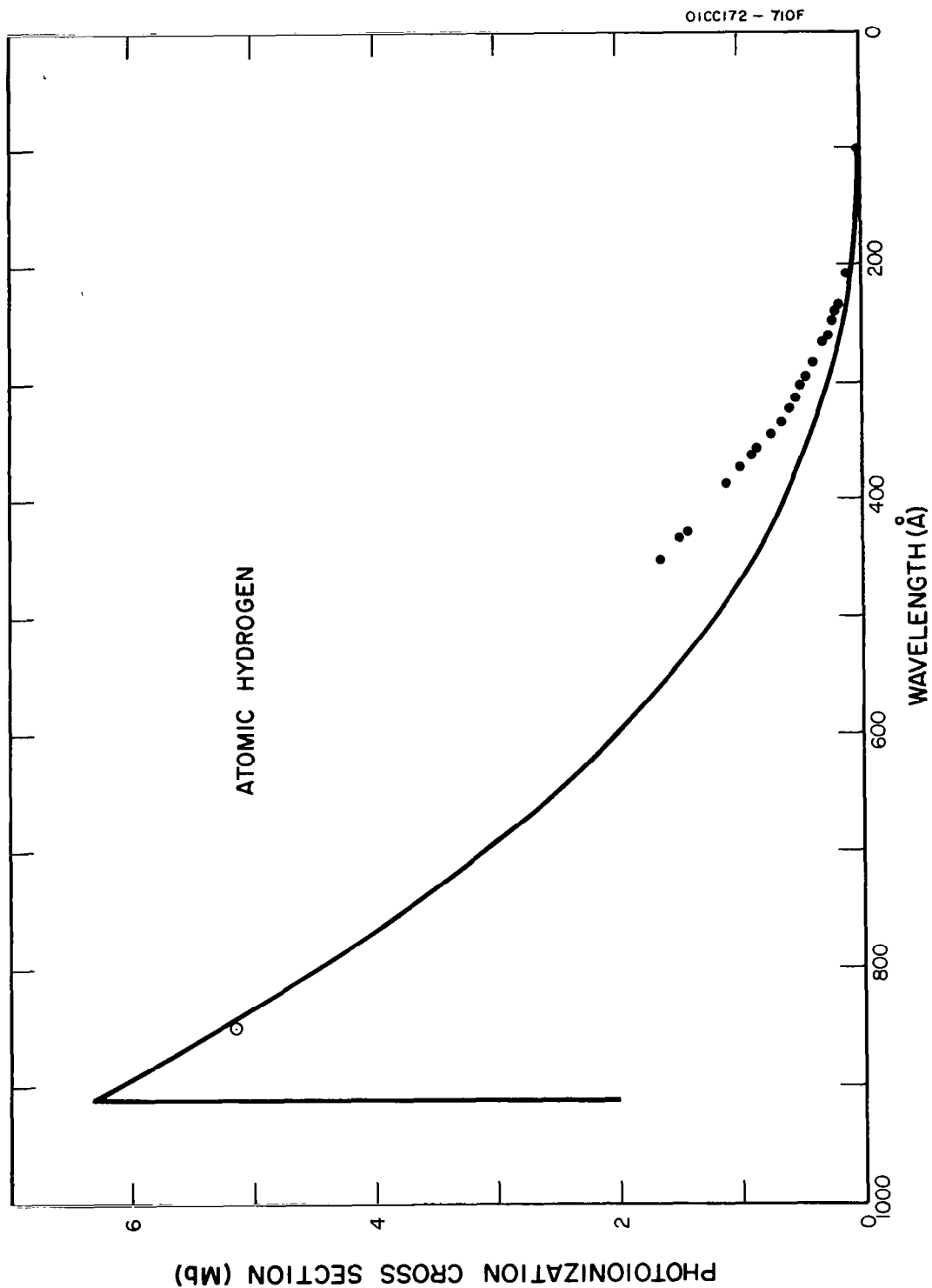
Figure 8. Theoretical photoionization cross section of atomic
hydrogen (solid line). Experimental points: ⊙ ,
Beynon and Cairns [11]; ● 1/2 σ (H₂) Samson and
Cairns [17].

TABLE 1

THEORETICAL CROSS SECTION OF ATOMIC HYDROGEN

$\lambda(\overset{\circ}{A})$	$\sigma(Mb)$	$\lambda(\overset{\circ}{A})$	$\sigma(Mb)$
1	2.09×10^{-8}	300	2.78×10^{-1}
2	2.28×10^{-8}	350	4.36×10^{-1}
4	2.51×10^{-8}	400	6.43×10^{-1}
6	9.87×10^{-7}	450	9.01×10^{-1}
8	2.62×10^{-6}	500	1.22×10^{-1}
10	5.55×10^{-6}	550	1.59×10^{-1}
20	5.56×10^{-5}	600	2.02×10^{-1}
30	2.10×10^{-4}	650	2.53×10^{-1}
40	5.39×10^{-4}	700	3.10×10^{-1}
50	1.10×10^{-3}	750	3.74×10^{-1}
75	4.02×10^{-3}	800	4.46×10^{-1}
100	9.92×10^{-3}	850	5.26×10^{-1}
150	3.47×10^{-2}	900	6.12×10^{-1}
200	8.33×10^{-2}	911.753	6.31×10^{-1}
250	1.62×10^{-1}	(threshold)	

1/2 $\sigma(H_2)$ is still about a factor of two greater than $\sigma(H)$. However, to shorter wavelengths, the ratio rapidly increases until at 1Å it is about 37:1. It is possible that this change in ratio is caused by the increased scattering cross section, which is not taken into account by Equation (17). Thus, although theory predicts the cross section for ionization of atomic hydrogen, the total attenuation of radiation at these short wavelengths is probably influenced more by the scattering cross section. (The Rayleigh scattering cross section σ_R of atomic hydrogen has been given by the expression

$$\sigma_R = \frac{1.143 \times 10^{-5} (2.253 \times 10^{-4})^2}{\lambda^4} , \qquad (18)$$

where λ is in Angstrom units [18]. Although this expression cannot legitimately be used within or in the neighborhood of a region of absorption, it is interesting to note that at 1Å, it would yield a cross section of 5.8×10^{-13} cm^2; cf. the theoretical photoionization cross section of 2.1×10^{-26} cm^2.)

The values of 1/2 $\sigma(H_2)$ between 200 and 450Å are given in Table 2, while those between 0.01 and 68Å are given in Table 3.

Oxygen

As in the case of hydrogen, the photoabsorption cross section of atomic oxygen could be determined using the equations developed earlier in this report if ground state molecules and atoms only were excited in the discharged gas. Reference to the potential energy curves of O_2 shown in Figure 9 shows that metastable molecules and atoms might be produced; for example, atomic oxygen exists in the metastable states ^1D and ^1S in addition to its ^3P ground

TABLE 2

ABSORPTION CROSS SECTIONS OF HYDROGEN ASSUMING $\sigma(H) = 1/2\ \sigma(H_2)$ [a]

$\lambda(\text{Å})$	$1/2\ \sigma(H_2)$ (Mb)	$\lambda(\text{Å})$	$1/2\ \sigma(H_2)$ (Mb)
209.3	0.13	323.6	0.61
234.2	.20	335.1	.68
239.6	.22	345.1	.76
247.2	.25	358.5	.88
260.5	.29	362.9	.92
266.3	.32	374.4	1.02
283.5	.40	387.4	1.13
297.6	.48	428.2	1.44
303.1	.51	434.3	1.51
314.9	.56	452.2	1.68

[a] Samson, J. A. R. and Cairns, R. B. (1965). Unpublished data.

TABLE 3

HYDROGEN ABSORPTION CROSS SECTIONS FROM .01 TO 68Å

$\lambda(\text{Å})$	Experimental [a] $\sigma(H) = 1/2\ \sigma(H_2)$ (Mb)	Semiempirical $\sigma(H)$ (Mb)	
.01	----	1.90×10^{-7}	Ref. b
.02	----	2.64×10^{-7}	Ref. b
.03	----	3.12×10^{-7}	Ref. b
.04	----	3.48×10^{-7}	Ref. b
.05	----	3.76×10^{-7}	Ref. b
.06	----	4.03×10^{-7}	Ref. b
.064	4.10×10^{-7}	----	
.072	4.18×10^{-7}	----	
.080	----	4.30×10^{-7}	Ref. b
.098	4.68×10^{-7}	----	
.100	----	4.67×10^{-7}	Ref. b
.130	5.35×10^{-7}	----	
.175	6.02×10^{-7}	----	
.200	6.27×10^{-7}	5.46×10^{-7}	Ref. b
.209	6.69×10^{-7}	----	
.260	6.27×10^{-7}	----	
.417	6.52×10^{-7}	----	
.497	7.28×10^{-7}	----	
.631	7.28×10^{-7}	----	
.710	7.28×10^{-7}	----	

TABLE 3 (continued)

$\lambda(\text{Å})$	Experimental [a] $\sigma(H) = 1/2\ \sigma(H_2)$ (Mb)	Semiempirical $\sigma(H)$ (Mb)	
.880	7.36×10^{-7}	----	
1.000	7.36×10^{-7}	6.57×10^{-7}	Ref. b
1.235	7.53×10^{-7}	----	
1.389	7.86×10^{-7}	----	
1.540	8.03×10^{-7}	----	
1.934	8.36×10^{-7}	----	
2.500	9.20×10^{-7}	----	
3.570	1.67×10^{-6}	----	
4.360	2.51×10^{-6}	----	
5.17	3.68×10^{-6}	----	
6.97	8.03×10^{-6}	----	
8.32	1.32×10^{-5}	1.25×10^{-5}	Ref. c
9.87	2.17×10^{-5}	----	
13.37	5.19×10^{-5}	5.02×10^{-5}	Ref. c
17.67	1.19×10^{-4}	1.17×10^{-4}	Ref. c
21.7	----	2.17×10^{-4}	Ref. c
23.7	----	2.84×10^{-4}	Ref. c
27.4	----	4.35×10^{-4}	Ref. c
31.6	----	6.70×10^{-4}	Ref. c
36.3	----	1.04×10^{-3}	Ref. c

TABLE 3 (continued)

$\lambda(\overset{\circ}{A})$	Experimental [a] $\sigma(H) = 1/2 \ \sigma(H_2)$ (Mb)	Semiempirical $\sigma(H)$ (Mb)	
44.6	1.67×10^{-3}	1.84×10^{-3}	Ref. c
68.0	5.02×10^{-3}	----	

[a] Determined from the mass absorption coefficients compiled by S. J. M. Allen in A. H. Compton and S. K. Allison, "X-Rays in Theory and Experiment," (D. Van Nostrand Co., Inc., N.Y., 1935), p. 799.

[b] Victoreen, J. A., (1949). J. Appl. Phys. 20, 1141.

[c] Henke, B. L., (1957). J. Appl. Phys. 28, 98.
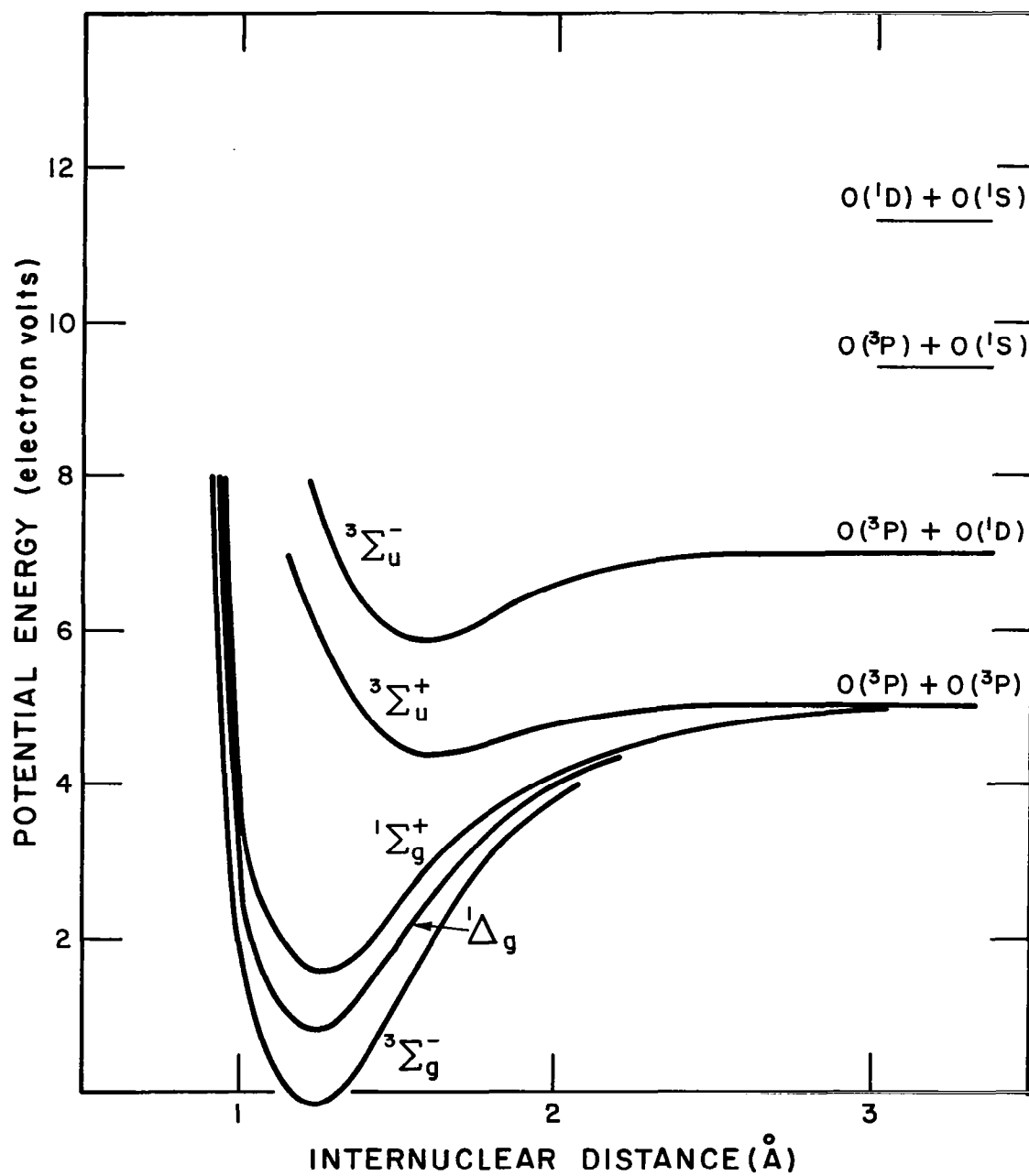
Figure 9. Potential energy curves for O_2.

state, and the $^1\Delta_g$ and $b^1\Sigma_g^+$ states of O_2 are known to be metastable. The relatively small amounts of energy, i.e., $\lesssim 3$ eV required to excite any one of these states would suggest that significant quantities of these species might be excited. The evidence in the literature concerning the state of the gas emerging from a discharge has been conflicting. For example, Linett and Marsden [19] have summarized work which suggested that the discharged gas consists mainly of ground state atoms and molecules. Fite and Brackmann [20] were unable to detect excited species in concentrations greater than 3 percent. However, Foner and Hudson [9] and subsequent workers [21] detected excited molecular species in considerable quantities. Most recently (indeed, since the completion of the measurements presented here), an important paper has been written by Huffman, et al. [22]. They identified nine allowed Rydberg series which converge to the three lowest states of O II; and in addition detected, by their absorption method, the presence of both metastable oxygen atoms and molecules downstream from a microwave discharge. The metastable molecules could be either in the $^1\Delta_g$ or $b^1\Sigma_g^+$ state, the former being regarded as the more likely. Bands originating from vibrationally excited ground state O_2 and line series owing to metastable oxygen atoms were very weak.

The apparatus used was similar to that employed in the hydrogen experiment. The major differences were that the absorption tube was only 30 cm long and the photodetector was a windowless photomultiplier (see Figure 10). The multiplier was maintained at a pressure of about 10^{-5} torr using a differential pumping section with 1 mm diameter holes drilled in its opposite faces to allow passage of the photon beam. With this geometry, a wavelength bandpass of 1.8Å was obtained.
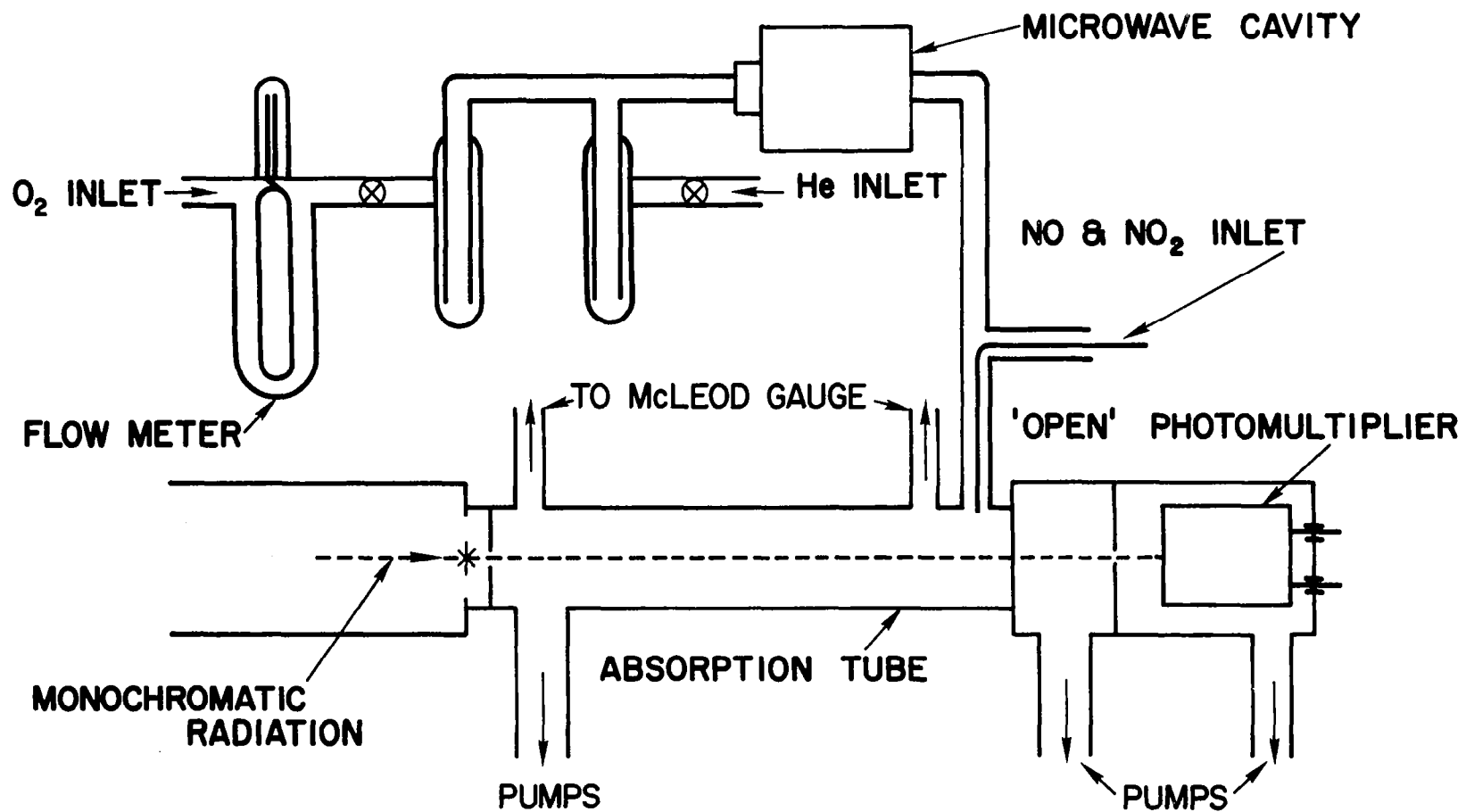
Figure 10.   Schematic diagram of absorption cell, photon detector, and gas inlet system.

The number density of the oxygen atoms was measured at the midpoint of the absorption cell using the nitrogen dioxide titration technique [23,24]. The decay of atoms along the cell, due to wall and volume recombination, was determined by adding nitric oxide to the gas stream. Nitric oxide recombines with atomic oxygen emitting visible radiation. Since the decreasing intensity of the visible radiation along the cell gave a direct measurement of the oxygen atom concentration gradient, the total number of absorbing atoms could be determined.

The degree of dissociation of molecular oxygen was promoted with two known techniques. First, traces of water vapor were not removed. Secondly, the oxygen was mixed with helium (the ratio was approximately four parts of helium to one part of oxygen). With no gas discharge, radiation with wavelengths shorter than 504Å was highly absorbed by $He(1^1S)$. At longer wavelengths, the absorption was characteristic of molecular oxygen in its ground state $O_2(^3\Sigma_g^-)$. With the discharge switched on, the absorption spectrum clearly showed the continued presence of both $O_2(^3\Sigma_g^-)$ and $He(1^1S)$. However, at certain wavelengths longer than 910Å, the ionization onset of atomic oxygen in its ground ^3P state, increased absorption was seen rather than the decrease expected since, at these wavelengths, the absorption cross section of $O(^3P)$ is zero. Consequently, other species were present. So that these species could be identified, the absorption cell was converted to serve both as an absorption cell and an ionization chamber, i.e., two fine nickel wire ion collectors were placed within the cell. Figures 11(a) through 11(e) show the results obtained.

Figure 11(a) shows the intensity of the radiation incident upon the absorbing gas measured as a function of wavelength. Figure 11(b) shows the
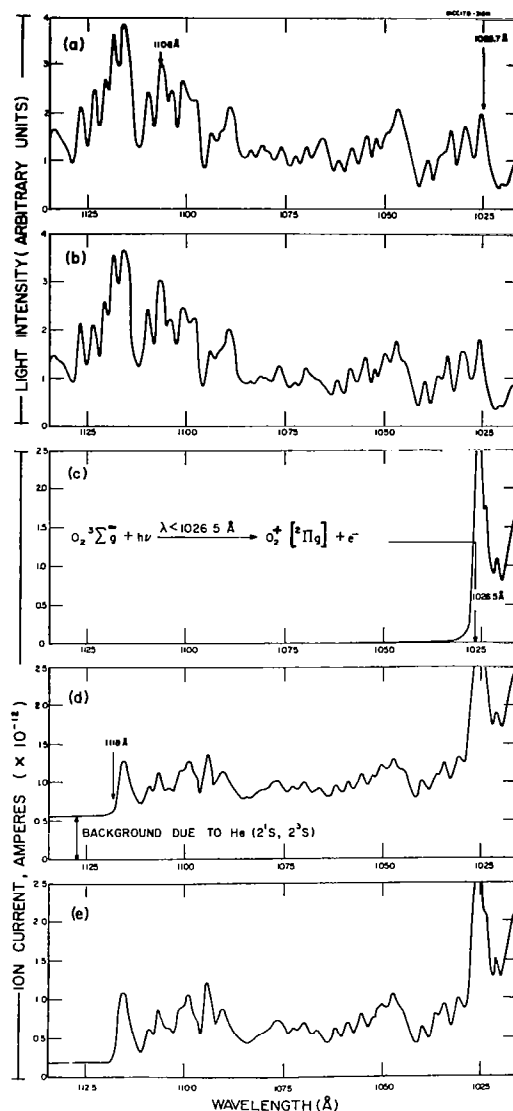
Figure 11. (a) The intensity of light incident upon the absorbing gas as a function of wavelength.

(b) The intensity of light transmitted by a $He(1^1S) - O_2(^3\Sigma_g^-)$ gas mixture as a function of wavelength.

(c) The current due to the photoionization of $O_2(^3\Sigma_g^-)$ as a function of wavelength.

(d) The current due to the photoionization of both $O_2(^3\Sigma_g^-)$ and $O_2(^1\Delta_g)$ as a function of wavelength.

(e) The current due to the photoionization of both $O_2(^3\Sigma_g^-)$ and $O_2(^1\Delta_g)$, as a function of wavelength, when oxygen atoms have recombined on a mercuric oxide surface.

intensity of the radiation transmitted by the He-O_2 gas mixture when there was no discharge. Figure 11(c) shows the ion current due to the photoionization process

$$O_2(^3\Sigma_g^-) + h\nu \rightarrow O_2^+(^2\Pi_g) + e^- \ . \tag{19}$$
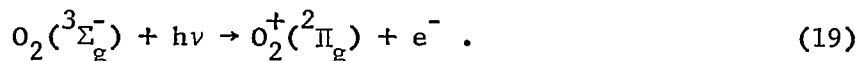
The conditions were the same as for 11(b), i.e., there was no discharge. The photoionization threshold of $O_2(^3\Sigma_g^-)$ is indicated. (More recent work has shown this threshold to occur at $1027.8 \pm 0.1\mathring{A}$ [25].)

Figure 11(d) shows the ion current when the He-O_2 gas mixture was discharged. The ionization threshold was shifted to a longer wavelength, indicating the presence of an additional species with an ionization potential 0.99 ± 0.04 eV less than that of ground state O_2. This energy difference is equal to the energy separation of the $^1\Delta_g$ and $^3\Sigma_g^-$ states of O_2. Thus, ionization at wavelengths shorter than $1118\mathring{A}$ was at least partially due to the process

$$O_2(^1\Delta_g) + h\nu \rightarrow O_2^+(^2\Pi_g) + e^- \ . \tag{20}$$
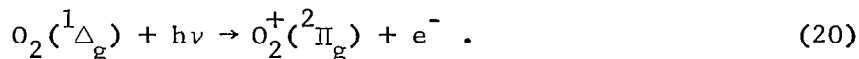
The conclusion that $^1\Delta_g$ molecules were formed within the discharge agrees with the papers previously referenced [9,21]. At wavelengths longer than $1118\mathring{A}$, there remained an appreciable ion current. Since the magnitude of this current was independent of wavelength, excited molecular states with energies greater than the $^1\Delta_g$ state (for example, the $^3\Sigma_u^+$ and $^1\Sigma_g^+$ states) could not have been present in measurable quantities. The constant current was ascribed to the ejection of electrons from the ion collectors by impacting metastable

helium atoms. This was confirmed with ion collectors of different geometries. Account had to be taken of the fact that metastable helium atoms can be ionized in this wavelength region. However, the ion current was reduced by less than 5 percent when the photon beam was switched off, showing that these metastables absorbed very little of the incident light.

The species identified in the discharged gas were, therefore, $O_2(^3\Sigma_g^-)$, $O_2(^1\Delta_g)$, $O(^3P)$, and ground state and metastable helium atoms. Oxygen atoms in the ^1D and ^1S states and ozone were assumed to be present in insufficient quantities to affect the cross section measurements. (This identification is in good accord with the spectroscopic results of Huffman, et al. [22].)

To determine the oxygen-atom cross section, it was necessary to remove selectively either the oxygen atoms or the $O_2(^1\Delta_g)$ molecules. Elias, et al. [21] have reported a means of obtaining this discrimination: oxygen atoms recombine rapidly on a mercuric oxide surface, but the $O_2(^1\Delta_g)$ molecules are not deactivated. A glass tube coated with mercuric oxide was placed in the flow system. It could be positioned either up or downstream from the discharge. In the upstream position, the atom and metastable concentrations were unaffected. In the downstream position, the mercuric oxide removed 97 percent of the oxygen atoms. (The glass tube was coated with mercuric oxide in the following manner: the tube was placed in a flow of discharged O_2. Upstream for the discharge, a pool of mercury was boiled such that the mercury vapor flowed through the discharge, see Figure 12.) The ion chamber was used firstly to confirm that the mercuric oxide did not deactivate $O_2(^1\Delta_g)$ molecules and secondly to indicate whether the oxygen atoms recombined to form ground

46
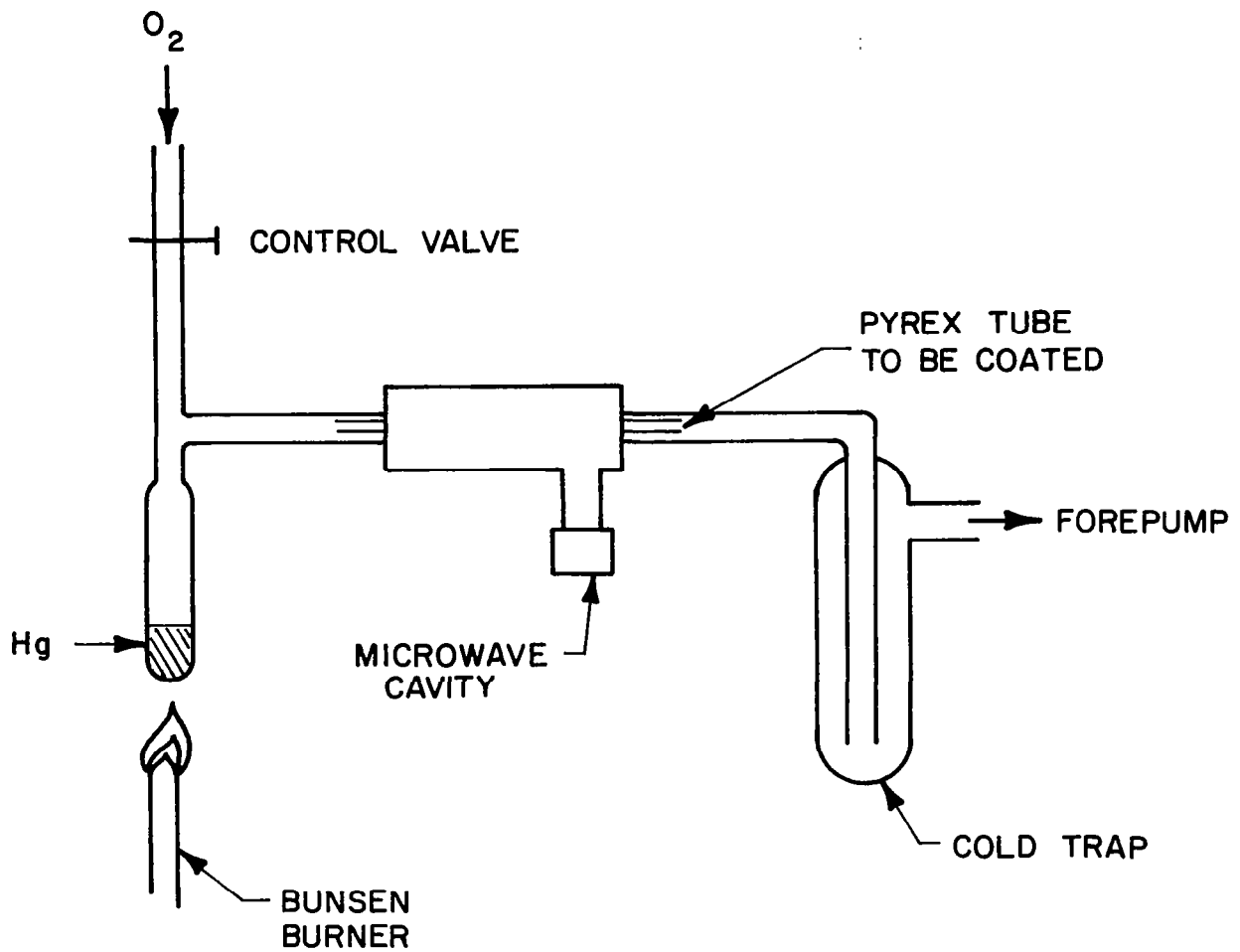
Figure 12.   System for coating tube with mercuric oxide.

state or excited oxygen molecules. Figure 11(e) shows the ion current measured with mercuric oxide downstream from the discharge. A comparison of Figures 11(d) and 11(e) shows that the mercuric oxide caused an increase in the $O_2(^1\Delta_g)$ concentration but deactivated about 70 percent of the metastable helium atoms. A fraction of the oxygen atoms must have recombined to form the additional $O_2(^1\Delta_g)$. Measurable quantities of more highly excited molecular states were not detected in the ion chamber. (States with a lifetime of less than 1×10^{-1} sec if formed on the mercuric oxide would not have reached the ion chamber.) At 1108Å, where the attenuation of the photon beam by both $O_2(^3\Sigma_g^-)$ and $O_2(^1\Delta_g)$ was small (the absorption cross section of $O_2(^3\Sigma_g^-)$ at this wavelength is $\simeq 0.0074 \times 10^{-18}$ cm^2) [26], the ratio of the ions produced before and after introduction of the mercuric oxide gave the ratio of the number densities of $O_2(^1\Delta_g)$ molecules. For the pressure range used in these experiments, the density of the $O_2(^1\Delta_g)$ molecules was increased 20 ± 4 percent when the oxygen atoms were recombined on the mercuric oxide surface.

The discharged gas contained $O_2(^3\Sigma_g^-)$, $O_2(^1\Delta_g)$, $O(^3P)$, $He(1^1S)$, and $[He(2^1S) - (2^3S)]$. Helium 1^1S atoms do not absorb at wavelengths longer than 504Å with the exception of the wavelengths corresponding to $1^1S - m^1P$ transitions. The 2^1S and 2^3S metastable helium atoms absorb continuously at wavelengths shorter than 3245 and 2610Å, respectively. Their absorption was, however, sufficiently weak to be neglected. Therefore, a measurement of the oxygen-atom photoabsorption cross section in the wavelength range 910 to 504Å had to take account only of $O_2(^3\Sigma_g^-)$, $O_2(^1\Delta_g)$, and $O(^3P)$.

With mercuric oxide upstream from the discharge, Equation (2) becomes:

$$\ln \frac{I_{(0,\lambda_1)}}{I'_{(\lambda_1)}} = L \left[\sigma_\lambda(O_2) \, N'(O_2) + \sigma_\lambda(O_2^*) \, N'(O_2^*) + \sigma_\lambda(O) \, N'(O) \right] , \quad (21)$$

where $\sigma_\lambda(O_2)$, $\sigma_\lambda(O_2^*)$, and $\sigma_\lambda(O)$ are the photoabsorption cross sections (cm^2) of $O_2(^3\Sigma_g^-)$, $O_2(^1\Delta_g)$, and $O(^3P)$, respectively; and $N'(O_2)$, $N'(O_2^*)$, and $N'(O)$ are the number densities (particles per cm^3) of $O_2(^3\Sigma_g^-)$, $O_2(^1\Delta_g)$, and $O(^3P)$, respectively.

With mercuric oxide downstream from the discharge, Equation (2) becomes:

$$\ln \frac{I_{(0,\lambda_1)}}{I''_{(\lambda_1)}} = L \left[\sigma_\lambda(O_2) \, N''(O_2) + \sigma_\lambda(O_2^*) \, N''(O_2^*) + \sigma_\lambda(O) \, N''(O) \right] \quad (22)$$

The different superscripts used in Equations (21) and (22) denote changes in the magnitude of $I'_{(\lambda_1)}$, $N'(O_2)$, $N'(O_2^*)$, and $N'(O)$.

Since the quantity of molecular oxygen flowing per second into the system remained constant,

$$N(O_2) = N'(O_2) + N'(O_2^*) + \frac{1}{2} N'(O) = N''(O_2) + N''(O_2^*) + \frac{1}{2} N''(O) . \quad (23)$$

where $N(O_2)$ was the number of oxygen molecules per cc when there was no discharge.

From Equations (21), (22), and (23),

$$\sigma_\lambda(O) = \frac{1}{2}\sigma_\lambda(O_2) - \frac{\frac{1}{L}\ln\frac{I'_\lambda}{I''_\lambda} + \left[\frac{N'(O_2^*) - N''(O_2^*)}{N''(O_2^*)}\right]\left[\frac{1}{L}\ln\frac{I_{(0,\lambda)}}{I''_{(\lambda)}} - N(O_2)\,\sigma_\lambda(O_2)\right]}{[N'(O) - N''(O)] - N''(O)\left[\frac{N'(O_2^*) - N''(O_2^*)}{N''(O_2^*)}\right]} \tag{24}$$

An experiment previously described in this paper showed that the number density of $O_2({}^1\Delta_g)$ molecules increased by 20 percent in the presence of mercuric oxide, i.e., $N''(O_2^*) \simeq \frac{6}{5}N'(O_2^*)$, therefore,

$$\frac{N'(O_2^*) - N''(O_2^*)}{N''(O_2^*)} = -\frac{1}{6}. \tag{25}$$

Equations (24) and (25) give an expression for $\sigma_\lambda(O)$ which involves measured quantities only; $I_{(0,\lambda)}$, $I'_{(\lambda)}$, and $I''_{(\lambda)}$ were measured with the windowless photomultiplier, $N'(O)$ and $N''(O)$ with the NO_2 titration technique, and $N(O_2)$ with a sensitive McLeod gauge. The effective length L of the absorbing gas column was assumed to equal the length of the absorption cell, i.e., no account was taken of both the viscous pressure drop and the pressure gradients at the ends of the cell. This assumption contributed to a total error in the determination of $\sigma_\lambda(O_2)$, estimated from a comparison with more accurate data previously obtained [27] of less than 10 percent. (Under all conditions, the calculated pressure difference between the ends of the cell due to viscous flow was less than 8 percent of the mean measured pressure.)

The estimated error in the determination of $\sigma_\lambda(O)$ was ± 30 percent. Values of this cross section are listed in Table 4.

TABLE 4

ABSORPTION CROSS SECTION OF ATOMIC OXYGEN

λ [Å]	$\sigma(O)$ [cm^2 x 10^{-18}]	λ [Å]	$\sigma(O)$ [cm^2 x 10^{-18}]
508.434 A III ⎱ 508.595 A III ⎰	13.3	725.542 A II	16.7
551.371 A VI	13.2	735.89 Ne I	14.3
584.331 He I	11.9	743.70 Ne I	7.6
585.754 A VII	12.3	758.677 O V 759.440 O V 760.229 O V 760.445 O V 761.130 O V 762.001 O V	8.3
624.617 O IV ⎱ 625.130 O IV 625.852 O IV ⎰	13.0	760.439 A IV	7.9
636.818 A III ⎱ 637.282 A III ⎰	13.7	774.522 O V	7.6
683.278 A IV	11.8	779.821 O IV ⎱ 779.905 O IV ⎰	11.1
684.996 N III 685.513 N III 685.816 N III 686.335 N III	17.3	822.159 A V	6.0
699.408 A IV ⎱ 700.277 A IV ⎰	12.7	832.754 O II 832.927 O III 833.326 O II 833.742 O III 834.462 O II	5.3
702.332 O III 702.822 O III 702.899 O III 703.850 O III	13.0	850.602	5.0
715.599 A V ⎱ 715.645 A V ⎰	12.2	901.168 A IV ⎱ 901.804 A IV ⎰	4.7

Discussion of Results. — The measured total absorption cross section of

atomic oxygen has been plotted in Figure 13 together with values of its ioni-

zation cross section obtained theoretically using both the dipole velocity and

dipole length formulations [28]. Dalgarno, et al. [28] favored the results

given by the dipole-velocity calculations, since the iterative process in-

volved converged more rapidly. In addition, the dipole-velocity calculation

was expected to be more accurate at short wavelengths [29].

The experimental points all lie above the preferred theoretical curve.

The measured cross section at 902Å, close to the photoionization threshold,

is about 50 percent higher than that calculated. The increase in cross sec-

tion obtained theoretically at 732Å and 665Å, due, respectively, to the added

possibilities of ionization to the ^2D or ^2P states of O^+, are not positively

confirmed by experiment. It is possible that these edges exist but are hidden

by absorption in line series going to the two series limits at 16.86 and 18.54

eV above the ground state of the oxygen atom. The more recent spectroscopic

data by Huffman, et al. [22], which will be discussed later, provide evidence

that this might indeed be the case. If an atom is excited to a discrete energy

state lying above its lowest ionization potential, it can de-excite with the

emission of radiation or, selection rules permitting, can undergo a radiation-

less transition to an adjoining continuum. In atomic oxygen, both of these

processes are possible. Thus, at certain wavelengths less than 910Å, all pho-

tons absorbed do not ionize atomic oxygen either by direct ionization or auto-

ionization. At these wavelengths, the total absorption cross section is greater

than the ionization cross section. At wavelengths where autoionization occurs,

the absorption lines are broadened and, if accounted for, could greatly alter

52
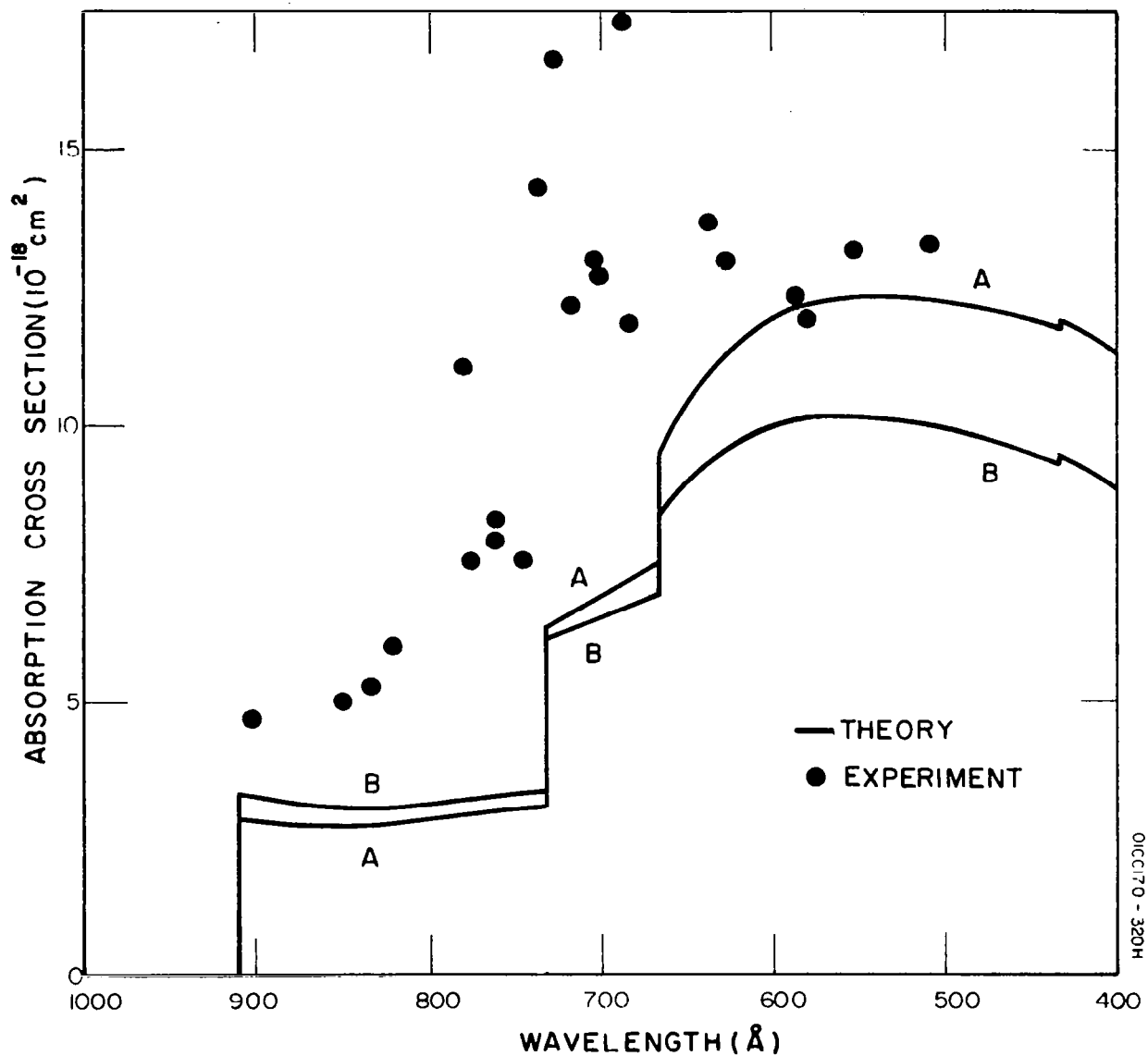
Figure 13. The absorption cross section of atomic oxygen, λ 1000 - λ 400Å. Curves A and B were computed using the dipole length and dipole velocity formulations respectively. The experimental points have an estimated accuracy of ±30 percent.

the computed photoionization cross section. These considerations could explain
the differences, which are largest at 780, 736, 725, and 686Å, between the ex-
perimental and calculated cross sections. This point has been clarified by
Huffman, _et al._ [30] who obtained the absorption spectrum of atomic oxygen and
found (as previously mentioned) nine Rydberg series due to _allowed transitions_
from the O^3P ground state. The upper states of these transitions are:

$$2s^2 \, 2p^3 \, (^4S^o) \, n \, s \quad ^3S^o \, ,$$

$$2s^2 \, 2p^3 \, (^4S^o) \, n \, d \quad ^3D^o \, ,$$

$$2s^2 \, 2p^3 \, (^2P^o) \, n \, s'' \, ^3P^o \, ,$$

$$^*2s^2 \, 2p^3 \, (^2P^o) \, n \, d'' \, ^3P^o \, ,$$

$$^*2s^2 \, 2p^3 \, (^2P^o) \, n \, d'' \, ^3D^o \, ,$$

$$2s^2 \, 2p^3 \, (^2D^o) \, n \, s' \, ^3D^o \, ,$$

$$^*2s^2 \, 2p^3 \, (^2D^o) \, n \, d' \, ^3S^o \, ,$$

$$2s^2 \, 2p^3 \, (^2D^o) \, n \, d' \, ^3P^o \, ,$$

$$^*2s^2 \, 2p^3 \, (^2D^o) \, n \, d' \, ^3D^o \, .$$

To quote Huffman, _et al._ [30]: "None of these series has been previously ob-
served in absorption in this wavelength region (600 to 960Å), and _the four_
series marked with asterisks were previously unknown. For two of the remain-
ing five series, only one member was known." Huffman, _et al._ [22] recently
completed a detailed analysis of the spectrum. A classification and listing
of these lines is reproduced in Tables 5 through 15. (The authors wish to
thank Dr. Huffman and his associates for permitting the reproduction of their
fine data prior to publication.) Huffman, _et al._ [30] compared the wavelengths
of atomic oxygen absorption lines with the wavelengths at which the cross sec-
tions were measured. Their comparison shows that at 685.5, 725.5, and 735.9Å,

54

TABLE 5[*]

SUMMARY OF ATOMIC OXYGEN SERIES. LOWER STATE IS OI GROUND STATE:

$$2s^2\, 2p^4\, {}^3P_2$$
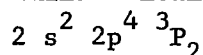
OII Level	Term Value [a] From OI Ground State ν(cm^{-1})	Convergence Limit λ(Å)	OI Series	Table
$2s^2\,2p^3\,({}^4S^o_{3/2})$	109837.03	910.440	$({}^4S^o)$ ns $\,{}^3S^o$	6
			$({}^4S^o)$ nd $\,{}^3D^o$	7
$2s^2\,2p^3\,{}^2D^o_{5/2}$	136645.4	731.821	$({}^2D^o)$ ns' $\,{}^3D^o$	8
$2s^2\,2p^3\,{}^2D^o_{3/2}$	136666.4	731.709	$({}^2D^o)$ nd' $\,{}^3S^o$	9
			$({}^2D^o)$ nd' $\,{}^3P^o$	10
			$({}^2D^o)$ nd' $\,{}^3D^o$	11
$2s^2\,2p^3\,{}^2P^o_{3/2}$	150303.9	665.319	$({}^2P^o)$ ns'' $\,{}^3P^o$	12
$2s^2\,2p^3\,{}^2P^o_{1/2}$	150305.4	665.312	$({}^2P^o)$ nd'' $\,{}^3P^o$	13
			$({}^2P^o)$ nd'' $\,{}^3D^o$	13
$2s\,2p^4$	--	--	$2s\,2p^5$ $\,{}^3P^o$	14

[*]Tables 5-15 have been compiled by Huffman, et al. [22] to whom all credit is due.

[a] See Eriksson, K. B. S., and Isberg, H. B. S., Arkiv Fysik 24, 549 (1963) for OII(^{4}S) and C. E. Moore, Atomic Energy Levels (N. B. S. Washington, 1949) Circular 467, Vol. 1, for difference between ^{4}S and ^{2}D or ^{2}P states of OII.

NOTE: Single and double prime on running electron designates terms converging to OII^{2}D and ^{2}P, respectively.

TABLE 6

OBSERVED OI ABSORPTION SERIES:
$$2s^2\, 2p^4\, {}^3P_{2,1,0} \;\rightarrow\; 2s^2\, 2p^3({}^4S^o_{3/2})ns\; {}^3S^o_1$$
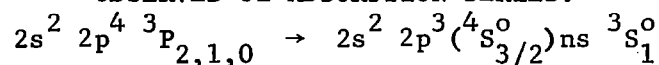
$n\ell$	J'', J'	$\lambda_{obs.}$ [f] (Å)	ν_{obs} [f] (cm^{-1})	$\nu_{Calc.}$ [a] (cm^{-1})	I[e]	Remarks
6 s	0,1	952.917	104940.9	38.4	1	
6 s	1,1	952.321	105006.6	06.4	1	
6 s	2,1	950.870	105166.8	64.9	3	
7 s	0,1	939.843	106400.7	01.4	2	
7 s	1,1	-	-	-	-	O_2 Band inter-
7 s	2,1	-	-	-	-	ference near emission line
8 s	1,1	931.618	107340.1	38.6	2	
8 s	2,1	930.241	107499.0	97.1	2	
10 s	1,1	-	-	-	-	near emission
10 s	2,1	922.200	108436.3	36.1	2	line
11 s	0,1	921.860	108476.3	80.8	3	blend; 9d,
11 s	1,1	921.247	108548.5	48.8	1	$J'' = 2$
11 s	2,1	919.908	108706.5	07.3	2	
12 s	1,1	919.559	108747.8		2	
12 s	2,1	918.221	108906.2		2	
13 s	2,1	916.960	109056.0		2	blend; 14d $J'' = 0$
14 s	1,1	917.315	109013.8		2	
14 s	2,1	915.991	109171.4		2	
15 s	2,1	915.199	109265.9		1	blend, 18d, $J'' = 0$
16 s	1,1	914.877	109185.0		3	blend, 16d, $J' = 0$; 13d, $J' = 2$
16 s	2,1	914.588	109338.8		3	
17 s	2,1	914.057	109402.4		1	blend; 20d, $J'' = 1$

TABLE 6 (cont.)

$n\ell$	J'', J'	$\lambda_{obs.}$[f] (Å)	ν_{obs}[f] (cm^{-1})	$\nu_{Calc.}$[a] (cm^{-1})	I[e]	Remarks
18 s	1,1	914.918	109299.4		2	blend; 17d,
18 s	2,1	913.644	109451.8		3	$J'' = 1$
19 s	2,1	913.250	109499.0		4	b
20 s	2,1	912.964	109533.3		4	b
21 s	2,1	912.723	109562.3		4	b
22 s	2,1	912.500	109589.0		3	b
23 s	2,1	912.318	109610.9		3	b
24 s	2,1	912.155	109630.5		3	b
25 s	2,1	912.012	109647.7		3	b
26 s	2,1	911.898	109661.4		2	b
27 s	2,1	911.786	109674.9		2	b
28 s	2,1	911.692	109686.2		2	b
29 s	2,1	911.611	109695.9		2	b
30 s	2,1	911.538	109704.7		2	b
31 s	2,1	911.463	109713.7		1	b
OII $^4S^o_{3/2}$ (Previous)			109837.03			c
OII $^4S^o_{3/2}$ (Present)			109836.6 ± 4.2			d

a. Calculated from atomic energy levels, C. E. Moore, Atomic Energy Levels (N.B.S. Washington, 1949), Circular 467, Vol. 1; first four digits same as previous column and omitted throughout Tables.

b. Blend with (n-1) d $^3D^o$; $J'' = 2$.

c. Edlen, B., Svenska Vetenskapsakad. Handl. 20, 3 (1943).

TABLE 6 (cont.)

d. Average from 22 $\Delta\nu$ values, $J'' = 2$.

e. Eye estimated intensity in this table and throughout paper.

f. Last digit should be subscripted. Estimated uncertainty is $\pm$ 0.02Å and $\pm$ 2 cm^{-1}.

TABLE 7

OBSERVED OI ABSORPTION SERIES:
$$2s^2\ 2p^4\ {}^3P_{2,1,0}\ \rightarrow\ 2s^2\ 2p^3\ ({}^4S^o_{3/2})nd\ {}^3D^o_{3,2,1}$$

$n\ell$	J''^a	$\lambda_{obs.}{}^f$ (Å)	$\nu_{obs}{}^f$ (cm^{-1})	$\nu_{Calc.}{}^b$ (cm^{-1})	I^e	Remarks
5 d	1	950.088	105253.4	50.1	2	
6 d	1	938.002	106609.6	07.3	2	
6 d	2	936.618	106767.1	65.8	3	
7 d	0	931.485	107355.5	56.2	2	
7 d	1	930.877	107424.2	24.2	2	
7 d	2	929.508	107583.8	82.7	3	
8 d	0	926.903	107886.1	90.1	2	
8 d	1	926.295	107957.0	58.1	3	
8 d	2	924.952	108113.7	16.6	2	
9 d	1	923.200	108318.9	19.3	3	
9 d	2	921.860	108476.3	77.8	3	blend, 11s,$J'' = 0$
10 d	0	921.575	108509.9	07.9	1	
10 d	1	921.005	108577.0	75.9	3	
10 d	2	919.658	108736.1	34.4	3	
11 d	0	919.971	108699.1		1	
11 d	1	919.376	108769.4		2	
11 d	2	918.039	108927.8		3	
12 d	0	918.724	108846.6		1	
12 d	1	918.149	108914.8		2	
12 d	2	916.816	109073.1		3	
13 d	1	917.185	109029		2	
13 d	2	915.877	109185.0		3	
14 d	0	916.960	109056.0		2	blend, 13s,$J'' = 2$
14 d	1	916.420	109120.3		3	
14 d	2	915.100	109277.7		2	
15 d	1	915.821	109191.7		3	
15 d	2	914.513	109347.8		3	

TABLE 7 (cont.)

$n\ell$	J'' [a]	$\lambda_{obs.}$ [f] (Å)	ν_{obs} [f] (cm^{-1})	$\nu_{Calc.}$ (cm^{-1})	I [e]	Remarks
16 d	1	915.321	109251.3		2	
16 d	2	913.997	109409.5		4	
17 d	0	915.499	109230.0		1	
17 d	1	914.918	109299.4		2	blend, 18s,$J''=1$
17 d	2	913.590	109458.3		3	
18 d	0	915.199	109265.9		1	blend, 15s,$J''=2$
18 d	1	914.588	109338.8		3	blend, 16s,$J''=2$
18 d	2	913.250	109499.0		4	c
19 d	0	914.854	109307.1		1	
19 d	1	914.293	109347.1		2	
19 d	2	912.964	109533.3		4	c
20 d	1	914.057	109402.4		3	blend, 17s,$J''=2$
20 d	2	912.723	109562.3		4	c
21 d	1	913.815	109431.3		3	
21 d	2	912.500	109589.0		3	c
22 d	1	913.644	109451.8		3	
22 d	2	912.318	109610.9		3	c
23 d	1	913.483	109471.1		3	
23 d	2	912.155	109630.5		3	c
24 d	2	912.012	109647.7		3	c
25 d	2	911.898	109661.4		2	c
26 d	1	913.127	109513.8		2	
26 d	2	911.786	109674.9		2	c
27 d	2	911.692	109686.2		2	c
28 d	2	911.611	109695.9		2	c
29 d	1	912.843	109547.9		3	
29 d	2	911.538	109704.7		2	c

TABLE 7 (cont.)

$n\ell$	J''[a]	$\lambda_{obs.}$[f] ($\overset{o}{A}$)	$\nu_{obs.}$[f] (cm^{-1})	$\nu_{Calc.}$ (cm^{-1})	I[e]	Remarks
30 d	2	911.463	109713.7		1	c
OII $^4S^o_{3/2}$ (Previous)			109837.03			d
OII $^4S^o_{3/2}$ (Present)			109836.8 ± 3.9			e

a. Upper state splitting not observed.

b. Calculated from levels in C. E. Moore, Atomic Energy Levels (N.B.S., Washington, 1949), Circular 467, Vol. 1; upper state splitting not observed.

c. Blend with $(n + 1)$ s $^3S^o_1$; $J'' = 2$.

d. Edlen, B., Kungl. Svenska Vetenskapsakad. Handl. 20, 3 (1943).

e. Average limit from 24 $\Delta\nu$ measurements; $J'' = 2$.

f. Last digit should be subscripted. Estimated uncertainty is $\pm 0.02\overset{o}{A}$ and ± 2 cm^{-1}.

TABLE 8

OBSERVED OI ABSORPTION SERIES:

$$2s^2\,2p^4\,{}^3P_{2,1,0} \;\rightarrow\; 2s^2\,2p^3\,({}^2D^o_{5\,2,\,3\,2})ns'\;{}^3D^o_{3,2,1}$$
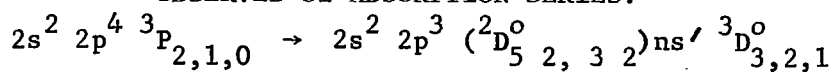
$n\ell$	J'',J'	$\lambda_{obs.}{}^c$ (Å)	$\nu_{obs.}{}^c$ (cm^{-1})	I	Remarks
4 s′	0,1	818.236	122214.1	7	
4 s′	1,2	817.835	122274.1	7	
4 s′	1,1	817.777	122282.7	7	
4 s′	2,3	816.862	122419.7	9	
4 s′	2,2	816.766	122434.1	9	
5 s′	0,1	776.569	128771.6	4	
5 s′	1,2	776.206	128831.8	5	
5 s′	1,1	776.159	128839.6	5	
5 s′	2,3	775.321	128978.8	7	
5 s′	2,2	775.252	128990.3	6	
6 s′	0,1	759.593	131649.4	3	
6 s′	1,2	759.262	131706.8	4	
6 s′	1,1	759.200	131717.6	3	
6 s′	2,3	758.412	131854.5	5	
6 s′	2,2	758.347	131865.8	4	
7 s″	0,1	750.956	133163.6	3	
7 s″	1,2	750.637	133220.2	3	
7 s″	1,1	750.573	133231.5	2	
7 s″	2,3	749.795	133369.8	3	
7 s″	2,2	749.742	133379.2	3	
8 s′	0,1	745.945	134038.1	2	
8 s′	1,2	745,628	134115.1	2	
8 s′	2,3	744.794	134265.3	7	blend, 7d′ ${}^3P^o$
9 s′	1,2	742.471	134685.4	2	
9 s′	2,3	741.625	134839.0	4	
10 s′	2,3	739.499	135226.7	3	
11 s′	2,3	737.995	135502.3	3	
12 s′	2,3	736.910	135701.8	3	

TABLE 8 (cont.)

$n\ell$	J'', J'	$\lambda_{obs.}{}^c$ (Å)	$\nu_{obs.}{}^c$ (cm^{-1})	I	Remarks
13 s$'$	2,3	736.092	135852.6	3	
OII $^2D_{5/2}^o$ (Previous)			136645.4		See Table 5
OII $^2D_{5/2}^o$ (Present)			136653.3 $\pm$ 12.0		a
OII $^2D_{3/2}^o$ (Previous)			136666.4		See Table 5
OII $^2D_{3/2}^o$ (Present)			136680.4 $\pm$ 13.8		b

(a) Upper states $^3D_3^o$ and $^3D_2^o$; average limit from 12 $\triangle\nu$ values

(b) Upper state $^3D_1^o$; average limit from 7 $\triangle\nu$ values

(c) Last digit should be subscripted. Estimated uncertainty is $\pm$0.02Å and $\pm$2 cm^{-1}

TABLE 9

OBSERVED OI ABSORPTION SERIES

$$2s^2\, 2p^4\, {}^3P_{2,1,0} \;\rightarrow\; 2s^2\, 2p^3\, ({}^2D^o_{5/2,3/2})\, nd'\, {}^3S^o_1$$
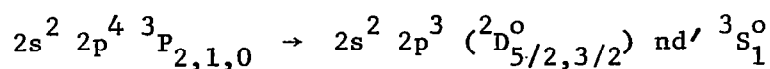
$n\ell$	J'', J	$\lambda_{obs.}{}^c$ (Å)	$\nu_{obs.}{}^c$ (cm^{-1})	I	Remarks
3 d'	0,1	805.745	124108.7	3	Blend 3d' ${}^3D^o$ $J''=J'=1$
3 d'	1,1	805.295	124178.1	7	
3 d'	2,1	804.267	124336.8	9	
4 d'	0,1	772.147	129509.0	2	
4 d'	1,1	771.729	129579.2	5	Diffuse
4 d'	2,1	770.793	129736.5	7	Diffuse
5 d'	1,1	757.149	132074.4	3	
5 d'	2,1	756.243	132232.6	6	
6 d'	0,1	749.894	133352.2	2	
6 d'	1,1	749.517	133419.3	3	
6 d'	2,1	748.632	133577.0	5	
7 d'	0,1	745.287	134176.5	2	
7 d'	1,1	744.899	134246.4	3	
7 d'	2,1	744.051	134399.4	6	
8 d'	1,1	742.062	134759.6	3	a
8 d'	2,1	741.177	134920.5	6	a
9 d'	1,1	740.053	135125.5	3	a
9 d'	2,1	739.188	135283.6	5	a
10 d'	1,1	738.644	135383.2	3	a
10 d'	2,1	737.779	135541.9	5	a
11 d'	1,1	737.614	135575.7	3	a
11 d'	2,1	736.134	135734.2	5	a
12 d'	1,1	736.824	135717.6	3	a
12 d'	2,1	735.960	135876.9	4	Near NeI line ; a
13 d'	1,1	736.219	135828.0	3	a
13 d'	2,1	735.367	135986.5	4	a
14 d'	1,1	735.760	135913.9	2	a
14 d'	2,1	734.913	136070.5	4	a

TABLE 9 (cont.)

$n\ell$	J'', J	$\lambda_{obs.}{}^{c}$ (Å)	$\nu_{obs.}{}^{c}$ (cm^{-1})	I	Remarks
15 d$''$	2, 1	734.544	136138.9	3	a
16 d$'$	1, 1	735.092	136037.4	2	a
16 d$'$	2, 1	734.251	136193.2	3	a
OII $^{2}D^{o}_{5/2}$ (Previous)			136645.4		See Table 5
OII $^{2}D^{o}_{5/2}$ (Present)			136642.5 $\pm$ 10.8		b

a. Blended with respective nd$'$ $^{3}D^{o}$ transitions.

b. Average limit from 22 $\Delta\nu$ values; predicted to converge to $^{2}D^{o}_{3/2}$ limit; see Huffman et al. [22].

c. Last digit should be subscripted. Estimated uncertainty is $\pm$ 0.02Å and $\pm$ 2 cm^{-1}.

TABLE 10

OBSERVED OI ABSORPTION SERIES

$$2\,s^2\,2p^4\,{}^3P_{2,1,0} \rightarrow 2\,s^2\,2p^3\,({}^2D^o_{5/2,3/2})\,nd',\,{}^3P^o_{2,1,0}$$
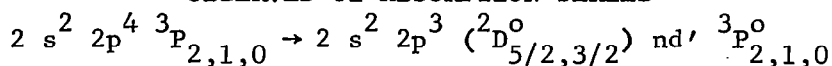
$n\ell$	J'',J'	$\lambda^e_{obs.}$ (Å)	$\nu^e_{obs.}$ (cm^{-1})	$\nu^a_{calc.}$ (cm^{-1})	I	Remarks
3 d'	0,1	812.154	123129.4	28.7	2	
3 d'	1,2	812.092	123138.8	38.1	2	
3 d'	1,1	811.696	123198.8	96.7	3	
3 d'	1,0	811.488	123230.4	28.4	3	
3 d'	2,2	811.051	123296.8	96.6	4	
3 d'	2,1	810.655	123357.0	55.2	3	
4 d'	0,1	770.690	129753.9	52.5	3	
4 d'	1,2	770.348	129811.5	11.1	3	
4 d'	1,1	770.271	129824.4	20.5	4	
4 d'	1,0	770.271	129824.4	25.7	4	
4 d'	2,2	769.411	129969.5	69.6	5	
4 d'	2,1	769.356	129978.8	79.0	4	
5 d'	0,1	757.059	132090.1	84[b]	3	
5 d'	1,2	756.704	132152.1	52	3	
5 d'	(1,1)(1,0)	756.663	132157.0	52	4	unresolved
5 d'	(2,2)(2,1)	755.790	132311.9	10	6	unresolved
	J''^c					
6 d'	0	749.628	133399.5	92[b]	3	
6 d'	1	749.253	133466.3	60	6	
6 d'	2	748.380	133622.0	18	6	
7 d'	0	745.159	134199.5		3	
7 d'	1	744.794	134265.3		7	blend, 8s' ${}^3D^o$
7 d'	2	743.929	134421.4		5	
8 d'	0	742.280	134720.1		3	
8 d'	1	741.914	134786.5		4	
8 d'	2	741.055	134942.8		5	
9 d'	0	740.313	135078.0		3	
9 d'	1	739.940	135146.1		4	
9 d'	2	739.085	135302.4		4	

66

TABLE 10 (continued)

$n\ell$	J''^c	$\lambda^e_{obs.}$ (Å)	$\nu^e_{obs.}$ (cm^{-1})	$\nu^a_{calc.}$ (cm^{-1})	I	Remarks
10 d'	0	738.906	135335.2		2	
10 d'	1	738.537	135402.8		4	
10 d'	2	737.683	135559.6		3	
11 d'	0	737.873	135524.7		3	
11 d'	1	737.495	135594.1		4	
11 d'	2	736.629	135753.5		3	
12 d'	0	737.083	135669.9		3	
12 d'	2	735.840	135899.1		2	
13 d'	0	736.460	135784.7		2	
13 d'	1	736.092	135852.6		3	
13 d'	2	735.234	136011.1		3	
14 d'	1	735.616	135940.5		3	
14 d'	2	734.746	136101.5		2	
15 d'	2	734.368	136171.5		2	
16 d'	2	733.987	136242.2		2	
OII	$^2D^o_{5/2}$	(Previous)	136645.4			See Table 5
OII	$^2D^o_{3/2}$	(Previous)	136666.4			See Table 5
OII	Limit	(Present)	136652.6 ± 8.9			d

a. Calculated from levels in C. E. Moore, Atomic Energy Levels (N.B.S. Washington, 1949) Circular 467, Vol. 1.

b. These levels not accurately known (B. Edler, Kungl. Svenska Veterskapsakad Handl. 20, 3 (1943).

c. Upper state splitting not resolved for these levels.

d. Average limit from 24 $\Delta\nu$ values with n > 4. Theory predicts $^3P^o_1$ and $^3P^o_o$ converge to $^2D^o_{5/2}$, and $^3P^o_2$ converges to $^2D^o_{3/2}$. No significant difference in limits found in this investigation. See Huffman, et al. [22].

e. Last digit should be subscripted. Estimated uncertainty is ±0.02Å and ±2 cm^{-1}.

TABLE 11

OBSERVED OI ABSORPTION SERIES

$$2\,s^2\,2p^4\,{}^3P_{2,1,0} \rightarrow 2\,s^2\,2p^3\,({}^2D^o_{5/2,3/2})\,nd'\,{}^3D^o_{3,2,1}$$
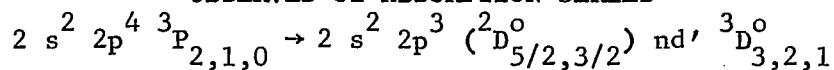
$n\ell$	J'',J'	$\lambda^d_{obs.}$ (Å)	$\nu^d_{obs.}$ (cm^{-1})	I	Remarks
3 d'	0,1	806.231	124033.9	4	
3 d'	1,2	805.810	124098.7	8	
3 d'	1,1	805.745	124108.7	3	
3 d'	2,3	804.848	124247.1	7	
3 d'	2,2	804.775	124258.3	6	
4 d'	0,1	772.344	129476.0	4	somewhat diffuse
4 d'	1,2	771.967	129539.2	6	diffuse
4 d'	2,3	771.056	129692.3	9	diffuse
5 d'	0,1	757.627	131991.1	3	
5 d'	1,2	757.254	132056.1	4	
5 d'	2,3	756.410	132203.4	6	
5 d'	2,2	756.354	132213.2	5	
6 d'	1,2	749.586	133407.0	3	
6 d'	2,3	748.680	133568.4	5	
	J''^a				
7 d'	1	745.011	134226.2	3	
7 d'	2	744.128	134385.2	5	
8 d'	1	742.062	134759.6	3	b
8 d'	2	741.177	134920.5	6	b
9 d'	1	740.053	135125.5	3	b
9 d'	2	739.188	135283.6	5	b
10 d'	1	738.644	135383.2	3	b
10 d'	2	737.779	135541.9	5	b
11 d'	1	737.614	135575.7	3	b
11 d'	2	736.734	135734.2	5	b
12 d'	1	736.824	135717.6	3	b
12 d'	2	735.960	135876.9	4	b, near NeI line

TABLE 11 (continued)

$n\ell$	J''[a]	$\lambda^d_{obs.}$ (Å)	$\nu^d_{obs.}$ (cm^{-1})	I	Remarks
13 d′	1	736.231	135828.0	3	b
13 d′	2	735.367	135986.5	4	b
14 d′	1	735.760	135913.9	2	b
14 d′	2	734.913	136070.5	4	b
15 d′	2	734.544	136138.9	3	b
16 d′	1	735.092	136037.4	2	b
16 d′	2	734.251	136193.2	3	b
OII	$^2D^o_{5/2}$	(Previous)	136645.4		See Table 5
OII	Limit	(Present)	136639.3 ± 7.7		c

a. Upper state splitting not observed for these transitions.

b. Blend with respective nd' $^3S^o_1$ transitions.

c. Average limit from 19 $\Delta\nu$ values. Theory predicts $^3D^o_{2,1}$ converge to $^2D^o_{5/2}$; $^3D^o_3$ to $^2D^o_{3/2}$. No significant difference in limit observed. See Huffman, et al. [22].

d. Last digit should be subscripted. Estimated uncertainty is ±0.02Å and ±2 cm^{-1}.

TABLE 12

OBSERVED OI ABSORPTION SERIES

$$2\ s^2\ 2p^4\ ^3P_{2,1,0} \rightarrow 2\ s^2\ 2p^3\ (^2P^o_{3/2,1/2})\ ns''\ ^3P^o_{2,1,0}$$
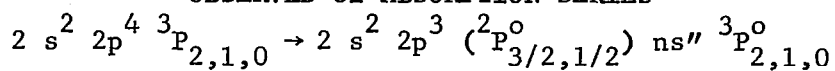
$n\ell$	J'',J'	$\lambda^e_{obs.}$ (Å)	$\nu^e_{obs.}$ (cm^{-1})	$\nu^a_{calc.}$ (cm^{-1})	I	Remarks
3 s″	0,1	879.529	113697.2	94.1	5	
3 s″	1,2	879.088	113754.3	51.7	4	
3 s″	1,1	879.007	113764.7	62.1	4	
3 s″	1,0	878.960	113770.8	68.3	4	
3 s″	2,2	877.876	113911.3	10.2	7	
3 s″	2,1	877.779	113921.3	20.6	8	
	J''[b]					
4 s″	2	737.019	135681.7		2	c
5 s″	2	701.014	142650.5		2	diffuse
6 s″	0	688.245	145297.1		2	diffuse
6 s″	1	687.997	145349.5		2	diffuse
6 s″	2	687.202	145517.6		4	diffuse
7 s″	1	680.866	146871.8		2	
7 s″	2	680.146	147027.3		2	
8 s″	1	676.763	147762.2		1	
8 s″	2	676.033	147921.8		2	
9 s″	2	673.421	148495.5		2	
10 s″	2	671.669	148882.9		2	
11 s″	2	670.425	149159.1		2	
12 s″	2	669.526	149359.4		2	
13 s″	2	668.832	149514.4		1	
14 s″	2	668.307	149631.8		1	
OII	$^2P^o_{3/2}$	(Previous)	150303.9			Table 5
OII	$^2P^o_{1/2}$	(Previous)	150305.4			Table 5
OII	Limit	(Present)	150305.6 ± 5.7			d

TABLE 12 (continued)

a. Calculated from levels in C. E. Moore, Atomic Energy Levels (N.B.S. Washington, 1949) Circular 467, Vol. 1.

b. Upper state splitting not observed.

c. Identification questionable. Level should be near OII $^2D^o$ limit and probably greatly perturbed by d' $^3P^o$ levels.

d. Average limit from 9 $\triangle \nu$ values between n = 5 to 13.

e. Last digit should be subscripted. Estimated uncertainty is $\pm 0.02 \overset{o}{A}$ and ± 2 cm^{-1}.

TABLE 13

OBSERVED OI ABSORPTION SERIES

$$2s^2 2p^4\ {}^3P_{2,1,0} \rightarrow 2s^2 2p^3 ({}^2P^o_{3/2,1/2})nd''\ {}^3P^o_{2,1,0}; nd''{}^3D^o_{3,2,1}$$

$n\ell$	J	$\lambda_{obs.}^{b}$ (Å)	$\nu_{obs.}^{b}$ (cm^{-1})	I	Remarks
3 d ${}^3P^o$	0	726.104	137721.3	3	Diffuse
3 d ${}^3P^o$	1	725.748	137788.9	4	Diffuse
3 d ${}^3P^o$	2	724.932	137944.0	5	Diffuse
3 d ${}^3D^o$	0	726.035	137734.4	3	less diffuse than ${}^3P^o$
3 d ${}^3D^o$	1	725.665	137804.6	5	less diffuse than ${}^3P^o$
3 d ${}^3D^o$	2	724.830	137963.4	6	less diffuse than ${}^3P^o$
$n\ell\ {}^3P^o,\ {}^3D^o$					
4 d	0	698.631	143137.1	3	Diffuse
4 d	1	698.297	143205.5	4	Diffuse
4 d	2	697.532	143362.5	6	Diffuse
5 d	0	686.603	145644.6	3	
5 d	1	686.284	145712.2	5	
5 d	2	685.544	145869.6	7	
6 d	0	680.256	147003.5	2	Diffuse
6 d	1	679.948	147070.1	4	Diffuse
6 d	2	679.202	147231.6	4	Diffuse
7 d	0	676.487	147822.5	2	Diffuse
7 d	1	676.183	147888.9	3	Diffuse
7 d	2	675.463	148046.6	5	Diffuse
8 d	2	673.052	148576.9	5	
9 d	0	672.404	148720.1	2	
9 d	1	672.090	148789.6	3	
9 d	2	671.406	148941.2	5	
10 d	1	670.952	149042.0	3	
10 d	2	670.237	149201.0	4	

TABLE 13 (Continued)

$n\ell$	J	$\lambda_{obs.}^{b}$ (A)	$\nu_{obs.}^{b}$ (cm^{-1})	I	Remarks
11 d	0	670.425	149159.1	2	
11 d	1	670.091	149233.4	2	
11 d	2	669.371	149394.0	4	
12 d	2	668.720	149539.4	4	
13 d	1	668.928	149492.9	1	
13 d	2	668.211	149653.3	3	
14 d	1	668.509	149586.6	2	
15 d	2	667.487	149815.6	3	
17 d	2	667.006	149923.7	3	
18 d	2	666.838	149961.5	2	
19 d	2	666.663	150000.8	1	
OII	$^2P^o_{3/2}$	(Previous)	150303.9		Table 5
OII	$^2P^o_{1/2}$	(Previous)	150305.4		Table 5
OII	Limit	(Present)	150303.8 ± 2.8		a

a. Average limit from 13 $\Delta\nu$ values with n > 4.

b. Last digit should be subscripted. Estimated uncertainty is ± 0.02Å and ± 2 cm^{-1}.

73

TABLE 14

OBSERVED OI MULTIPLET

$$2\,s^2\,2p^4\,^3P_{2,1,0} \to 2\,s\,2p^5\,^3P^o_{2,1,0}$$

J'',J'	$\lambda^b_{obs.}$ (Å)	$\nu^b_{obs.}$ (cm^{-1})	$\nu^a_{calc.}$ (cm^{-1})	I	Remarks
1,2	792.951	126111.2	08.0	6	Blend
0,1	792.951	126111.2	13.4	6	Blend
1,1	792.501	126182.8	81.4	4	
1,0	792.231	126225.8	24.9	4	
2,2	791.966	126268.0	66.5	7	
2,1	791.508	126341.1	39.9	5	

a. Calculated from energy levels, Ref. C. E. Moore, Atomic Energy Levels, (N.B.S. Washington, 1949) Circular 467, Vol. 1.

b. Last digit should be subscripted. Estimated uncertainty is ±0.02Å and ±2 cm^{-1}.

TABLE 15

OBSERVED TRIPLET TERMS OF OI. EFFECTIVE QUANTUM NUMBERS n^* AND QUANTUM DEFECTS μ CALCULATED FROM LIMITS INDICATED USING R = 109733.55 cm^{-1} FOR OXYGEN.[a] LIMITS ARE THOSE GIVEN IN TABLE 5.

Symbol	E(cm^{-1})[b]	ΔE	n^*	μ	Remarks
Configuration: $2s^2 2p^4$					
$2p^4\ ^3P_2$	0.00	158.29			Ref. a
$2p^4\ ^3P_1$	158.29				Ref. a
$2p^4\ ^3P_0$	226.99	68.70			Ref. a
Configuration: $2s^2 2p^3\ (^4S^o_{3/2})\ ns\ ^3S^o_1$; Limit: 109837.03 cm^{-1}					
6 s $^3S^o_1$	105166.5		4.8472	1.1528	65.244 Ref. a
7 s $^3S^o_1$	106627.7		5.8474	1.1526	27.946 Ref. a
8 s $^3S^o_1$	107498.7		6.8505	1.1495	97.236 Ref. a
9 s $^3S^o_1$	108056.0		7.8494	1.1506	57.6 Ref. b
10 s $^3S^o_1$	108436.3		8.8511	1.1489	36.1 Ref. b
11 s $^3S^o_1$	108705.3		9.8470	1.1530	07.3 Ref. b
12 s $^3S^o_1$	108906.1		10.857	1.143	
13 s $^3S^o_1$	109056.0		11.853	1.147	
14 s $^3S^o_1$	109171.7		12.843	1.157	
15 s $^3S^o_1$	109265.9		13.859	1.141	
16 s $^3S^o_1$	109341.0		14.874	1.126	
17 s $^3S^o_1$	109402.4		15.890	1.110	
18 s $^3S^o_1$	109454.7		16.942	1.058	
19 s $^3S^o_1$	109499.0		18.018	0.982	
20 s $^3S^o_1$	109533.3		19.008	0.992	

TABLE 15 (continued)

Symbol	$E(cm^{-1})^{b'}$	ΔE	n^*	μ	Remarks
Configuration: $2s^2\,2p^3\,(^4S^o_{3/2})\,ns\;^3S^o_1$; Limit: $109837.03\ cm^{-1}$					
21 s $^3S^o_1$	109562.3		19.987	1.013	
22 s $^3S^o_1$	109589.0		21.035	0.965	
23 s $^3S^o_1$	109610.5		22.01	0.99	Blend: (n-1) d $^3D^o$
24 s $^3S^o_1$	109631.0		23.08	0.92	Blend: (n-1) d $^3D^o$
25 s $^3S^o_1$	109647.7		24.08	0.92	Blend: (n-1) d $^3D^o$
26 s $^3S^o_1$	109661.4		25.00	1.00	Blend: (n-1) d $^3D^o$
27 s $^3S^o_1$	109673.5		25.91	1.09	Blend: (n-1) d $^3D^o$
28 s $^3S^o_1$	109686.2		26.98	1.02	Blend: (n-1) d $^3D^o$
29 s $^3S^o_1$	109695.9		27.89	1.11	Blend: (n-1) d $^3D^o$
30 s $^3S^o_1$	109705.4		28.88	1.12	Blend: (n-1) d $^3D^o$
31 s $^3S^o_1$	109713.7		29.83	1.17	Blend: (n-1) d $^3D^o$
Configuration: $2s^2\,2p^3\,(^4S^o_{3/2})\,nd\;^3D^o\;{}^{d'}$; Limit: $109837.03\ cm^{-1}$					
5 d $^3D^o$	105411.7		4.9796	0.0204	09.020 Ref. a
6 d $^3D^o$	106767.5		5.9791	0.0201	65.815 Ref. a
7 d $^3D^o$	107583.1		6.9775	0.0225	82.789 Ref. a
8 d $^3D^o$	108114.0		7.9804	0.0196	16.6 Ref. b
9 d $^3D^o$	108476.7		8.9816	0.0184	77.8 Ref. b
10 d $^3D^o$	108736.1		9.9838	0.0162	34.4 Ref. b
11 d $^3D^o$	108927.2		10.982	0.018	
12 d $^3D^o$	109073.3		11.984	0.016	
13 d $^3D^o$	109186.3		12.986	0.014	

TABLE 15 (continued)

Symbol	$E(cm^{-1})^{b'}$	ΔE	n^*	μ	Remarks
Configuration: $2s^2\,2p^3\,(^4S^o_{3/2})\,nd\ ^3D^o\ a'$; Limit: $109837.03\ cm^{-1}$					
14 d $^3D^o$	109279.7		14.032	-0.032	
15 d $^3D^o$	109348.9		15.649	-0.649	
16 d $^3D^o$	109409.5		16.021	-0.021	
17 d $^3D^o$	109457.6		17.007	-0.007	
18 d $^3D^o$	109496.3		17.95	0.05	
19 d $^3D^o$	109533.2		19.01	-0.01	
20 d $^3D^o$	109563.1		20.02	-0.02	
21 d $^3D^o$	109589.3		21.05	-0.05	
22 d $^3D^o$	109610.5		22.01	-0.01	Blend: (n+1) s $^3S^o$
23 d $^3D^o$	109631.0		23.08	-0.08	Blend: (n+1) s $^3S^o$
24 d $^3D^o$	109647.7		24.08	-0.08	Blend: (n+1) s $^3S^o$
25 d $^3D^o$	109661.4		25.00	0.00	Blend: (n+1) s $^3S^o$
26 d $^3D^o$	109673.5		25.91	0.09	Blend: (n+1) s $^3S^o$
27 d $^3D^o$	109686.2		26.98	0.02	Blend: (n+1) s $^3S^o$
28 d $^3D^o$	109695.9		27.89	0.11	Blend: (n+1) s $^3S^o$
29 d $^3D^o$	109705.4		28.88	0.12	Blend: (n+1) s $^3S^o$
30 d $^3D^o$	109713.7		29.83	0.17	Blend: (n+1) s $^3S^o$

TABLE 15 (continued)

Symbol	$E(cm^{-1})^{b'}$	ΔE	n^*	μ	Remarks
Configurations: $2s^2 p^3 (^2D^o_{5/2}) ns'$, $^3D^o_{3,2}$; Limit: 136645.4 cm^{-1}					
$2s^2 p^3 (^2D^o_{3/2}) ns'$, $^3D^o_1$; Limit: 136666.4 cm^{-1}					
4 s' $^3D^o_3$	122419.7	13.5	2.7774	1.2226	
$^3D^o_2$	122433.2		2.7788	1.2212	
$^3D^o_1$	122441.0	7.8	2.7774	1.2226	
5 s' $^3D^o_3$	128978.8		3.7833	1.2167	
$^3D^o_2$	128990.2	11.4	3.7861	1.2139	
$^3D^o_1$	128998.2	8.0	3.7829	1.2171	
6 s' $^3D^o_3$	131854.5		4.7859	1.2141	
$^3D^o_2$	131865.5	11.0	4.7914	1.2086	
$^3D^o_1$	131876.1	10.6	4.7862	1.2138	
7 s' $^3D^o_3$	133369.8		5.7879	1.2121	
$^3D^o_2$	133378.8	9.0	5.7959	1.2041	
$^3D^o_1$	133390.2	11.4	5.7874	1.2126	
8 s' $^3D^o_3$	134265.3		6.7900	1.2100	
$^3D^o_2$	134273.4	8.1	6.8016	1.1984	
$^3D^o_1$	134285.1	11.7	6.7883	1.2117	
9 s' $^3D^o_3$	134839.0		7.7940	1.2060	
$^3D^o_2$	134843.7	4.7	7.8042	1.1958	
10 s' $^3D^o_3$	135226.7		8.7948	1.2052	
11 s' $^3D^o_3$	135502.3		9.798	1.202	
12 s' $^3D^o_3$	135701.8		10.784	1.216	
13 s' $^3D^o_3$	135852.6		11.765	1.235	

TABLE 15 (continued)

Symbol	$E(cm^{-1})^{b'}$	ΔE	n^*	μ	Remarks

Configuration: $2s^2 2p^3 (D^o_{5/2})\, nd'\; ^3S^o_1$; Limit: $136645.4\; cm^{-1}$

Symbol	$E(cm^{-1})^{b'}$	ΔE	n^*	μ	Remarks
3 d' $^3S^o_1$	124336.3		2.9858	0.0142	
4 d' $^3S^o_1$	129736.6		3.9854	0.0146	
5 d' $^3S^o_1$	132232.6		4.9867	0.0133	
6 d' $^3S^o_1$	133577.9		5.9810	0.0190	
7 d' $^3S^o_1$	134402.5		6.9946	0.0054	
8 d' $^3S^o_1$	134919.2		7.9730	0.0270	Blend: nd' $^3D^o$
9 d' $^3S^o_1$	135283.7		8.977	0.023	Blend: nd' $^3D^o$
10 d' $^3S^o_1$	135541.7		9.971	0.029	Blend: nd' $^3D^o$
11 d' $^3S^o_1$	135734.1		10.973	0.027	Blend: nd' $^3D^o$
12 d' $^3S^o_1$	135876.4		11.946	0.054	Blend: nd' $^3D^o$
13 d' $^3S^o_1$	135986.4		12.904	0.096	Blend: nd' $^3D^o$
14 d' $^3S^o_1$	136071.3		13.825	0.175	Blend: nd' $^3D^o$
15 d' $^3S^o_1$	136138.9		14.719	0.281	Blend: nd' $^3D^o$
16 d' $^3S^o_1$	136194.4		15.598	0.402	Blend: nd' $^3D^o$

Configuration: $2s^2 2p^3 (^2D^o_{3/2})\, nd'\; ^3P^o_{2,1,0}$; Limit: $136666.4\; cm^{-1}$

Symbol	$E(cm^{-1})^{b'}$	ΔE	n^*	μ	Remarks
3 d' $^3P^o_2$	123297.0		2.8649	0.1351	96.6 Ref. b
$^3P^o_1$	123356.8	59.8	2.8714	0.1286	55.2 Ref. b
$^3P^o_0$	123388.7	31.9	2.8748	0.1252	86.9 Ref. b
4 d' $^3P^o_2$	129969.7		4.0480	-0.0480	69.60 Ref. b
$^3P^o_1$	129980.8	11.1	4.0513	-0.0513	79.04 Ref. b
$^3P^o_0$	129982.7	1.9	4.0519	-0.0519	84.15 Ref. b

79

TABLE 15 (continued)

Symbol	$E(cm^{-1})^{b'}$	ΔE	n^*	μ	Remarks
Configuration: $2\,s^2\,2p^3\,(^2D^o_{3/2})\,nd'\,^3P^o_{2,1,0}$; Limit: $136666.4\ cm^{-1}$					
5 d' $^3P^o_2$	132311.1		5.0197	-0.0197	10 Ref. b
$^3P^o_1$	132316.2	5.2	5.0224	-0.0224	
6 d' $^3P^o_2$	133622.0		6.0041	-0.0041	18 Ref. b
$^3P^o_1$	133626.5	4.5	6.0085	-0.0085	
7 d' $^3P^o_2$	134421.4		6.9914	0.0086	
$^3P^o_1$	134426.5	5.1	6.9993	0.0007	
8 d' $^3P^o_2$	134943.8		7.9814	0.0086	
$^3P^o_1$	134947.1		7.9890	0.0110	
9 d' $^3P^o_2$	135303.5		8.9730	0.0270	
$^3P^o_1$	135305.0	1.5	8.9779	0.0221	
10 d' $^3P^o_2$	135560.3		9.960	0.040	
$^3P^o_1$	135562.2	1.9	9.969	0.031	
11 d' $^3P^o_2$	135752.9		10.960	0.040	
$^3P^o_1$	135751.7	1.2	10.953	0.047	
12 d' $^3P^o_2$	135899.1		11.959	0.041	
$^3P^o_1$	135896.9	-2.2	11.942	0.058	
13 d' $^3P^o_2$	136011.0		12.940	0.060	
$^3P^o_1$	136011.7	-0.7	12.946	0.054	
14 d' $^3P^o_2$	136100.1		13.920	0.080	
15 d' $^3P^o_2$	136171.5		14.891	0.109	
16 d' $^3P^o_2$	136242.2		16.084	-0.084	

TABLE 15 (continued)

Symbol	$E(cm^{-1})^{b'}$	ΔE	n^*	μ	Remarks

Configuration: $2s^2 2p^3 (^2D^o_{5/2})$ nd' $^3D^o_{3,2,1}$; Limit: 136645.4 cm^{-1}

Symbol	$E(cm^{-1})^{b'}$	ΔE	n^*	μ	Remarks
3 d' $^3D^o_3$	124247.1		2.9750	0.0240	
$^3D^o_2$	124257.7	10.6	2.9763	0.0237	
$^3D^o_1$	124264.0	6.3	2.9770	0.0230	
4 d' $^3D^o_3$	129692.3		3.9727	0.0273	
$^3D^o_2$	129697.5	5.2	3.9741	0.0259	
$^3D^o_1$	129703.0	5.5	3.9757	0.0243	
5 d' $^3D^o_3$	132203.4		4.9703	0.0297	
$^3D^o_2$	132213.8	10.4	4.9761	0.0239	
$^3D^o_1$	132218.1	4.3	4.9785	0.0215	
6 d' $^3D^o$	133566.8		5.9703	0.0297	
7 d' $^3D^o$	134385.0		6.9675	0.0325	
8 d' $^3D^o$	134919.2		7.9730	0.0270	Blend: nd' $^3S^o_1$
9 d' $^3D^o$	135283.7		8.9770	0.0230	Blend: nd' $^3S^o_1$
10 d' $^3D^o$	135541.7		9.9711	0.0289	Blend: nd' $^3S^o_1$
11 d' $^3D^o$	135734.1		10.973	0.027	Blend: nd' $^3S^o_1$
12 d' $^3D^o$	135876.4		11.946	0.054	Blend: nd' $^3S^o_1$
13 d' $^3D^o$	135986.4		12.904	0.096	Blend: nd' $^3S^o_1$
14 d' $^3D^o$	136071.3		13.825	0.175	Blend: nd' $^3S^o_1$
15 d' $^3D^o$	136138.9		14.719	0.281	Blend: nd' $^3S^o_1$
16 d' $^3D^o$	136194.4		15.598	0.402	Blend: nd' $^3S^o_1$

TABLE 15 (continued)

Symbol	$E(cm^{-1})^{b'}$	ΔE	n^*	μ	Remarks

Configuration: $2s^2 2p^3 ({}^2P^o_{3/2,1/2})\, ns''\ {}^3P^o_{2,1,0}$; Average Limit: 150304.7 cm^{-1}

Symbol	$E(cm^{-1})^{b'}$	ΔE	n^*	μ	Remarks
$3\ s''\ {}^3P^o_2$	113911.9		1.7364	1.2636	10.20 Ref. b
${}^3P^o_1$	113922.8	10.9	1.7367	1.2633	20.63 Ref. b
${}^3P^o_0$	113929.1	6.3	1.7369	1.2631	26.80 Ref. b
$4\ s''\ {}^3P^o_0$	(135681.7)		(2.7394)	(1.2606)	Perturbed, nd' ${}^3P^o$ series
$5\ s''\ {}^3P^o$	142650.5		3.786	1.214	
$6\ s''\ {}^3P^o$	145513.1		4.783	1.217	
$7\ s''\ {}^3P^o$	147028.7		5.788	1.212	
$8\ s''\ {}^3P^o$	147921.1		6.785	1.215	
$9\ s''\ {}^3P^o$	148495.5		7.788	1.212	
$10\ s''\ {}^3P^o$	148882.9		8.785	1.215	
$11\ s''\ {}^3P^o$	149159.1		9.787	1.213	
$12\ s''\ {}^3P^o$	149359.4		10.774	1.226	
$13\ s''\ {}^3P^o$	149514.4		11.784	1.216	
$14\ s''\ {}^3P^o$	149631.8		12.770	1.230	

Configuration: $2s^2 2p^3 ({}^2P^o_{3/2,1/2})\, nd''\ {}^3P^o, {}^3D^o\ a'$; Average Limit: 150304.7 cm^{-1}

Symbol	$E(cm^{-1})^{b'}$	ΔE	n^*	μ	Remarks
$3\ d''\ {}^3P^o$	137946.5		2.9798	0.0202	
$3\ d''\ {}^3D^o$	137962.5		2.9818	0.0182	
$4\ d''\ {}^3P^o, {}^3D^o$	143363.4		3.9760	0.0240	
$5\ d''\ {}^3P^o, {}^3D^o$	145870.5		4.9746	0.0254	
$6\ d''\ {}^3P^o, {}^3D^o$	147230.1		5.9741	0.0259	

TABLE 15 (continued)

Symbol	$E(\text{cm}^{-1})^{b'}$	ΔE	n^*	μ	Remarks

Configuration: $2s^2 2p^3 \, (^2P^o_{3/2,1/2})$ nd″ $^3P^o, ^3D^o$ a′; Average Limit: 150304.7 cm⁻¹

Symbol	$E(\text{cm}^{-1})^{b'}$	ΔE	n^*	μ	Remarks
7 d″ $^3P^o, ^3D^o$	148047.7		6.9727	0.0273	
8 d″ $^3P^o, ^3D^o$	148576.9		7.9694	0.0306	
9 d″ $^3P^o, ^3D^o$	148945.4		8.9849	0.0151	
10 d″ $^3P^o, ^3D^o$	149200.6		9.969	0.041	
11 d″ $^3P^o, ^3D^o$	149390.6		10.957	0.043	
12 d″ $^3P^o, ^3D^o$	149539.4		11.974	0.026	
13 d″ $^3P^o, ^3D^o$	149652.0		12.962	0.038	
14 d″ $^3P^o, ^3D^o$	149744.9		14.001	-0.001	
15 d″ $^3P^o, ^3D^o$	149815.6		14.979	0.021	
17 d″ $^3P^o, ^3D^o$	149923.7		16.971	0.029	
18 d″ $^3P^o, ^3D^o$	149961.5		17.881	0.119	
19 d″ $^3P^o, ^3D^o$	150000.8		19.002	-0.002	

Configuration: $2s \, 2p^5 \, {}^3P^o_{2,1,0}$

Symbol	$E(\text{cm}^{-1})^{b'}$	ΔE	n^*	μ	Remarks
$2p^5 \, {}^3P^o_2$	126268.7			66.48	Ref. b
		71.5			
${}^3P^o_1$	126340.2			39.92	Ref. b
		43.9			
${}^3P^o_0$	126384.1			83.44	Ref. b

a′ Multiplet splittings for these terms too small to be observed.

b′ Last digit should be subscripted. Estimated uncertainty ± 2 cm⁻¹.

a. K·B·S· Eriksson and H·B S Isberg, Arkiv Fysik 24, 549 (1963)

b. C·E Moore, Atomic Energy Levels (NBS, Washington, 1949) Circular 467, Vol. 1

where high absorption cross sections were obtained, there would be appreciable absorption by discrete transitions in atomic oxygen. However, no line absorption was seen at 780Å, where a relatively high absorption cross section was obtained. It seems probable, therefore, that the measured absorption cross section at 780Å was too high.

A possible source of this increased absorption is suggested below. The change in the absorptance of the discharged gas which occurred when the mercuric oxide coated tube was moved from a position upstream to one downstream from the microwave discharge was ascribed mainly to atomic oxygen. An additional change might have occurred. If the mercuric oxide were regarded as a source of Hg vapor, it is possible that with the coated tube upstream from the discharge, Hg ions were produced in the discharge and reached the absorption cell. This could not have occurred with the mercuric oxide downstream from the discharge. Kelley [31] has listed a mercury transition at 779.83Å but does not give the energy levels or the ion (i.e., Hg II, III, or IV) involved. This transition coincides almost exactly in wavelength with the O IV emission line from the spark source (779.82Å). If allowance is made for the width of the emission line, it is apparent that an appreciable overlap could result, with a corresponding enhancement in absorption. Huffman, et al. [30] draw attention to the fact that if the large absorption cross sections which are due to atomic line absorption are omitted, the measured data show a definite step increase in cross section with decreasing wavelength in the region of the $O^+ \, ^2D^o$ state threshold which is similar to the theoretical curve. The energy level diagram of atomic oxygen compiled by Huffman, et al. to include transitions having wavelengths longer than 680Å is reproduced in Figure 14.

Figure 14. Atomic oxygen energy level diagram. Compiled by Huffman, et al [22].

At the 584Å He I line prominent in the solar spectrum, the measured cross section is 11.9×10^{-18} cm^2. This is in good agreement with the value given by Dalgarno and Parkinson [32] and subsequently used in discussions of the formation of the Earth's ionosphere.

In the X-ray region, the ionization cross section of atomic oxygen has been assumed to equal $1/2 \; \sigma(O_2)$. This assumption cannot be arbitrarily extended to longer wavelengths. However, $1/2 \; \sigma(O_2)$ measured over the wavelength range 300 to 200Å (Table 16(a)) shows close agreement with the dipole length calculation [28]. Measurements of $\sigma(O_2)$ in this region have been reported by several authors [33,34,35]. Excellent agreement was obtained with the work of Po Lee [35]. In Table 16(b) are values of $1/2 \; \sigma(O_2)$ listed from 0.01 to 68Å.

Finally in Table 17 are listed the theoretical scattering and absorption cross sections of Woo and Sun [36] for wavelengths between 0.064 and 8.32Å.

Appendix I. — In addition to the absorption cross section of atomic oxygen, the experiment described gave both the product $N(O_2^*) \; \sigma(O_2^*)$ and information as to whether $\sigma(O_2^*)$ was greater or less than $\sigma(O_2)$. A technique for measuring $N(O_2^*)$ has been discussed by Elias, et al. [21]. Thus, the absorption cross section of the $O_2(^1\Delta_g)$ molecule could be measured. Elias, et al. [21] found, in agreement with Foner and Hudson [9] and Herron and Schiff [37], that about 10 percent of discharged oxygen is in the $^1\Delta_g$ state. If this is so, the fraction f of oxygen atoms recombining on the mercuric oxide surface to form $O_2(^1\Delta_g)$ can be calculated, since

$$N''(O_2^*) - N'(O_2^*) = \frac{1}{2} \, f[N'(O) - N''(O)] . \tag{26}$$

TABLE 16(a)

ABSORPTION CROSS SECTIONS OF OXYGEN ASSUMING $\sigma(O) = 1/2 \ \sigma(O_2)$ [a]

$\lambda(\text{Å})$	$1/2 \ \sigma(O_2)$ (Mb)	$\lambda(\text{Å})$	$1/2 \ \sigma(O_2)$ (Mb)
209.3	4.5	323.6	8.4
225.2	5.3	335.1	8.4
234.2	5.3	345.1	8.5
239.6	6.0	362.9	8.8
247.2	6.2	374.4	9.0
266.3	7.0	387.4	9.3
283.5	7.6	428.2	9.7
303.1	8.7	434.3	9.8
314.9	8.2		

[a] Samson, J. A. R. and Cairns, R. B. [25].

TABLE 16(b)

OXYGEN ABSORPTION CROSS SECTIONS FROM .01 TO 68Å

Shell	λ(Å)	Experimental [a] $\sigma(O) = 1/2\ \sigma(O_2)$ (Mb)	Semiempirical $\sigma(O)$ (Mb)	
K	.01	----	1.52×10^{-6}	Ref. b
	.02	----	2.11×10^{-6}	Ref. b
	.03	----	2.50×10^{-6}	Ref. b
	.04	----	2.80×10^{-6}	Ref. b
	.05	----	3.02×10^{-6}	Ref. b
	.06	----	3.24×10^{-6}	Ref. b
	.064	3.45×10^{-6}	----	
	.072	3.64×10^{-6}	----	
	.080	----	3.56×10^{-6}	Ref. b
	.098	3.83×10^{-6}	----	
	.100	----	3.83×10^{-6}	Ref. b
	.130	4.16×10^{-6}	----	
	.175	4.50×10^{-6}	----	
	.200	4.87×10^{-6}	5.02×10^{-6}	Ref. b
	.260	5.58×10^{-6}	----	
	.417	9.89×10^{-6}	----	
	.497	1.38×10^{-5}	----	
	.631	2.39×10^{-5}	----	
	.710	3.23×10^{-5}	----	
	.880	5.84×10^{-5}	----	

TABLE 16(b)   (continued)

Shell	$\lambda(\text{Å})$	Experimental [a] $\sigma(O) = 1/2\ \sigma(O_2)$ (Mb)	Semiempirical $\sigma(O)$ (Mb)	
K	1.000	8.36×10^{-5}	8.75×10^{-5}	
	1.235	1.52×10^{-4}	----	
	1.389	2.15×10^{-4}	----	
	1.540	2.97×10^{-4}	----	
	1.934	5.84×10^{-4}	----	
	2.50	1.21×10^{-3}	----	
	3.57	3.99×10^{-3}	----	
	4.36	6.86×10^{-3}	----	
	5.17	1.10×10^{-2}	----	
	6.97	2.59×10^{-2}	----	
	8.32	4.22×10^{-2}	4.10×10^{-2}	Ref. c
	9.87	7.12×10^{-2}	----	
	13.37	1.45×10^{-1}	1.44×10^{-1}	Ref. c
	17.67	2.65×10^{-1}	2.86×10^{-1}	Ref. c
	21.7	----	4.40×10^{-1}	Ref. c
	23.3	----	----	
L	23.3	----	----	
	23.7	----	2.60×10^{-2}	Ref. c
	27.4	----	3.90×10^{-2}	Ref. c
	31.6	----	4.30×10^{-2}	Ref. c

TABLE 16(b)   (continued)

Shell	$\lambda(\text{Å})$	Experimental [a] $\sigma(0) = 1/2\ \sigma(0_2)$ (Mb)	Semiempirical $\sigma(0)$ (Mb)	
L	36.3	----	8.40×10^{-2}	Ref. c
	44.6	1.54×10^{-1}	----	
	68.0	4.30×10^{-1}	----	

[a] Determined from the mass absorption coefficients compiled by S. J. M. Allen in A. H. Compton and S. K. Allison, "X-Rays in Theory and Experiments," (D. Van Nostrand Co., Inc., N.Y., 1935), p. 799.

[b] Victoreen, J. A., (1949). J. Appl. Phys. 20, 1141.

[c] Henke, B. L., (1957). J. Appl. Phys. 28, 98.

TABLE 17

OXYGEN: TOTAL ABSORPTION (σ_t) AND SCATTERING (σ_s) CROSS SECTIONS [a]

Shell	$\lambda(\overset{\circ}{A})$	σ_t(Mb)	σ_s(Mb)
K	.064	3.1×10^{-6}	3.1×10^{-6}
	.098	3.7×10^{-6}	3.6×10^{-6}
	.130	4.1×10^{-6}	4.0×10^{-6}
	.260	5.8×10^{-6}	4.9×10^{-6}
	.417	1.00×10^{-5}	5.7×10^{-6}
	.631	2.27×10^{-5}	6.9×10^{-6}
	.710	3.04×10^{-5}	7.4×10^{-6}
	1.000	7.70×10^{-5}	9.2×10^{-6}
	1.235	1.42×10^{-4}	1.09×10^{-5}
	1.540	2.74×10^{-4}	1.31×10^{-5}
	1.934	5.43×10^{-4}	1.60×10^{-5}
	2.500	1.18×10^{-3}	1.99×10^{-5}
	3.570	3.42×10^{-3}	2.77×10^{-5}
	5.170	9.97×10^{-3}	3.98×10^{-5}
	6.970	2.414×10^{-2}	5.08×10^{-5}
	8.320	4.069×10^{-2}	5.71×10^{-5}

[a] Woo, Y. H. and Sun, C. P. (1937-47). "On the Absorption of X-Rays," Nat. Tsing Hua Univ. Sci. Rep., A4, 398.

from Equation (25),

$$N'(O_2^*) = \frac{5}{2} f [N'(O) - N''(O)] = \frac{1}{10} N(O_2) .$$ (27)

Therefore,

$$f = \frac{N(O_2)}{25[N'(O) - N''(O)]} ,$$ (28)

and when values of $N(O_2)$, $N'(O)$, and $N''(O)$ are substituted, $f \approx 0.2$.

Appendix II. — McNeal and Cook [38] have recently noted that the ionization potential of $O_2(^3\Sigma_g^-)$ can be found by adding the known energy of the transition $O_2 (a^1\Delta_g \rightarrow X^3\Sigma_g^-)$ to the observed ionization threshold of the $O_2(^1\Delta_g)$ molecule. Their work confirmed the fact that the ionization threshold of $O_2(^1\Delta_g)$ is 1118.0Å (11.09 eV). Adding this energy to that of the above transition, namely 0.977 eV [39], the ionization potential of $O_2(^3\Sigma_g^-)$ is found to be 12.067 eV. This is in close agreement with the value of 12.063 ± 0.001 eV measured recently by Samson and Cairns [25].

Nitrogen

The experiments so far described, involving H and O atoms, illustrate the problems which are produced by the presence of species in the discharged gas other than ground state molecules and atoms. Much literature exists describing the state of the gas emerging from discharged nitrogen. As a result, great difficulty was anticipated in the measurement of the absorption cross section of atomic nitrogen. This, in fact, was the case, and data have not been obtained.

In this brief report, a survey of data published on nitrogen afterglows is given, and emphasis is placed on the identification of species in the discharged gas. No attempt has been made to compile a complete bibliography. A discussion is given of the single previous experimental attempt to measure $\sigma(N)$ [40] and the results are compared with theories [41,42,32]. Also, a new series attributed to transitions from the $^4S^o$ ground state of the nitrogen atom to Rydberg terms $2s2p^3(^5S^o)np: \ 4^P$ [43] is mentioned and the wavelength of the transitions tabulated. The experimental work is then described and the results discussed.

The Composition of Nitrogen Afterglows. — Various types of nitrogen afterglows have been reported which differ in their durations, their spectra, and their sensitivity to gaseous contaminants. These afterglows have been surveyed (see, for example, Mitra [44] and Oldenberg [45]).

No attempt will be made to discuss the mechanisms responsible for these features, but mention will be made of the excited species which have been identified in the nitrogen afterglow. Species expected to be present might include nitrogen molecules (in vibrationally excited levels of the ground electronic state and in excited metastable electronic states), molecular ions, and atomic nitrogen in both its metastable and ground electronic states. The potential energy curves of N_2 are shown in Figure 15. Metastable N_2 molecules include the singlet level $N_2(a^1\Pi_g)$ (the upper level of the Lyman-Birge-Hopfield bands), which has a natural lifetime of the order of 1.7×10^{-4} sec (Lichten [46]) and the $A^3\Sigma_u^+$ level (the upper level of the Vegard-Kaplan bands), which is extremely insensitive to collisional deactivation in the presence of N_2 [47,48]. In
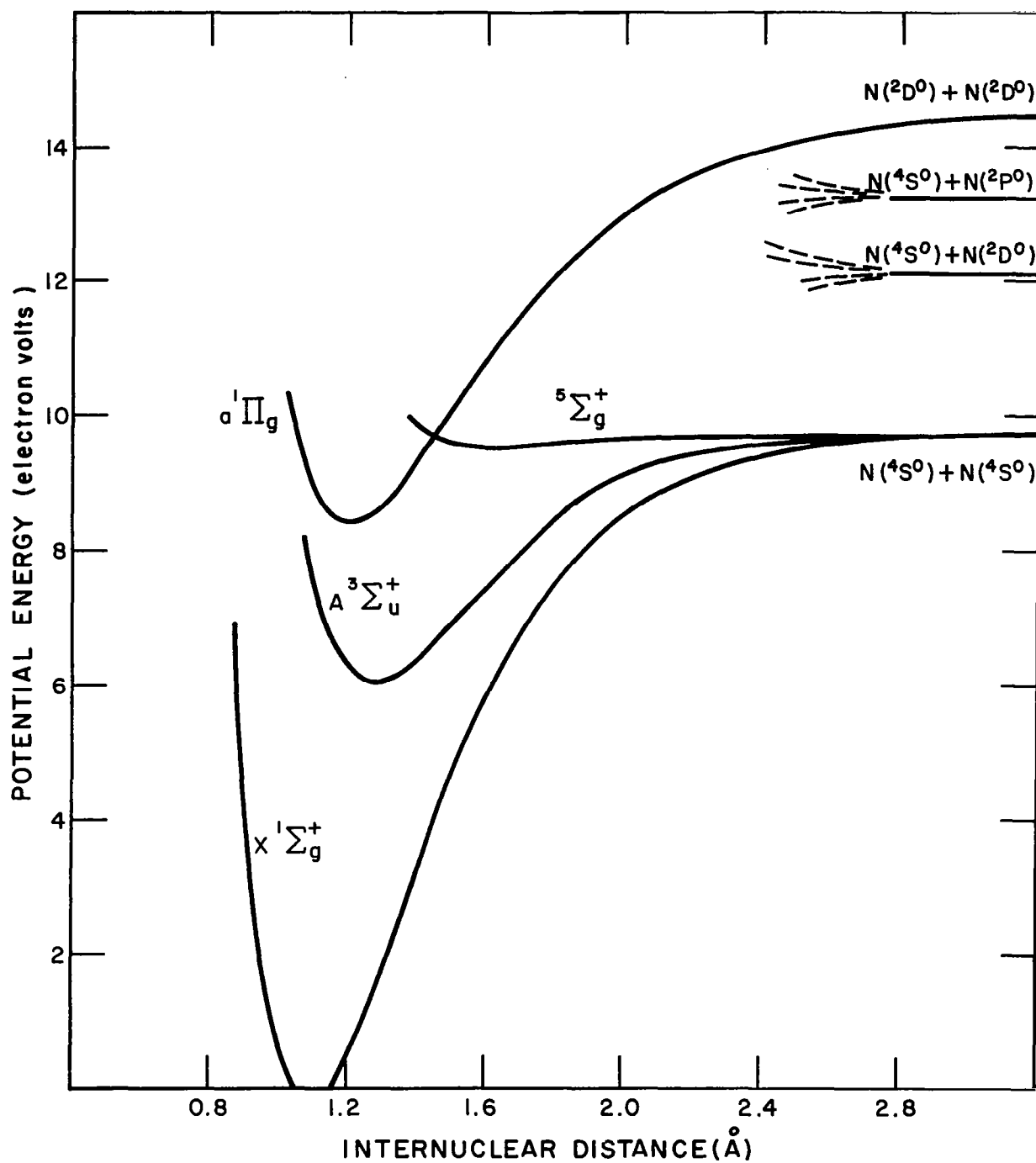
Figure 15. Selected potential energy curves for N_2.

addition, vibrationally excited $N_2(X^1\Sigma_g^+)$ levels from which radiative transitions are forbidden have been detected in nitrogen afterglows (for example, see Bass [49] and Ogawa, et al. [50]). Bass reported that more than 10 percent of the nitrogen existed in levels of vibrational excitation higher than $v = 8$.

Nitrogen molecules can be dissociated to form $2p^3\ ^4S$ ground state atoms or either of the metastable $2p^3\ ^2D$ or $2p^3\ ^2P$ states (see Figure 15). The relative abundances of these species have been estimated by Tanaka, et al. [51] whose results are reproduced below in Table 18. It can be seen that the concentrations of the metastable atoms are negligible.

Mitra [44] concluded that N_2^+ ions were present and an important constituent in nitrogen afterglows. This view does not receive support from the fact that the glows cannot be quenched by an electric field.

The Experiment of Ehler and Weissler. — Ehler and Weissler [40] discharged N_2 in a Phillips ionization gauge discharge and measured the absorption cross sections of the composite discharged gas, both during the discharge and its afterglow. On the basis of a number of simplifying assumptions, it was concluded that ground state N_2 and N were the only strongly absorbing species in the wavelength range 700 to 400Å. Hence, the absorption cross sections of atomic nitrogen could be determined. The results obtained are shown in Figure 16. Reasonable agreement was obtained with the theoretical data of Bates and Seaton [41]. At wavelengths longer than 750Å, Ehler and Weissler state that, "Experimental values were obtained but not indicated in the figures, σ_p (the absorption cross section of the plasma) was sometimes less than, sometimes

TABLE 18

CONCENTRATION OF $N(^4S)$ IN THE FIRST STAGES OF THE AFTERGLOW[*]

Pressure N_2 (mm Hg)	Pressure Argon (mm Hg)	$\dfrac{\text{Pressure } N(^4S)}{\text{Pressure } N_2} \times 100$
3.05		0.08
1.58		0.11
5.55		0.09
1.20		0.11
1.98		0.12
0.32	7.88	0.55
0.42	8.00	0.63
0.52	7.58	0.40
1.44	7.57	0.28
0.55	8.50	0.27
0.80	8.20	0.23

$$\frac{\text{Pressure } N(^2P)}{\text{Pressure } N_2} \cong \frac{1}{500} \times \frac{\text{Pressure } N(^4S)}{\text{Pressure } N_2}$$

and Pressure $N(^2D) \lesssim$ Pressure $N(^2P)$

[*]From Tanaka, et al., Planet. and Sp. Sci. 1, 7 (1959).
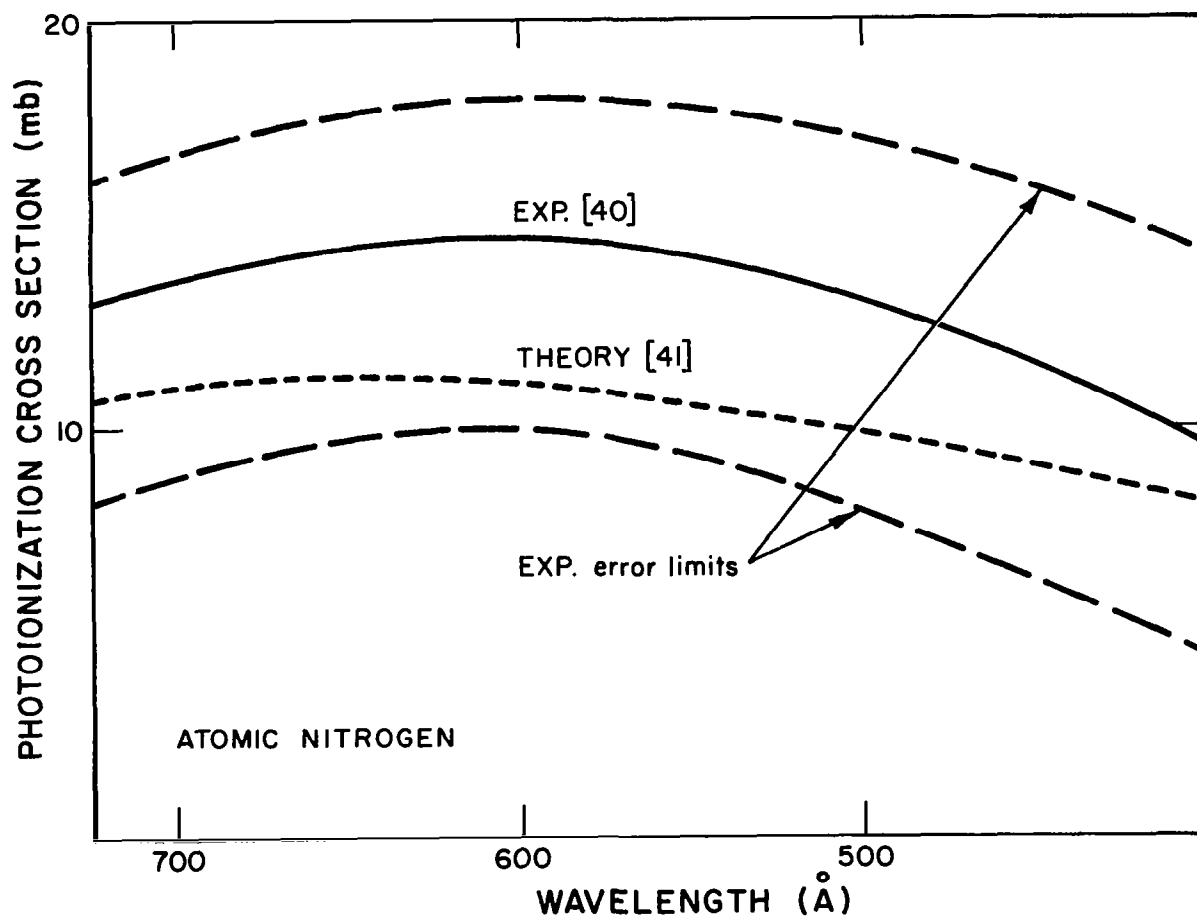
Figure 16. Atomic nitrogen photoionization cross section.

greater than, and sometimes equal to σ_{N_2} in a random manner which has been found characteristic of band absorption." However, if σ_p were greater than σ_{N_2} at any wavelength longer than 853Å (excluding Rydberg series transitions) species other than ground state N_2 and N must have been causing appreciable absorption. This conclusion is based on the knowledge that, at these wavelengths, the absorption cross section of atomic nitrogen is zero. This together with the fact that Ehler and Weissler did not measure the nitrogen atom concentration renders the data uncertain but nevertheless valuable as an order of magnitude estimate.

Theoretical Estimates. — The theoretical calculations of Bates and Seaton [41] gave the cross sections $\sigma(N)$ at the ionization onset resulting from both the dipole length and velocity approximations. The values were 10.2 and 7.7 Mb, respectively. Using a more approximate treatment based on the dipole length formulation, they computed the variation in cross section with wavelength, neglecting the absorption due to the inner shell electrons. Dalgarno and Parkinson [32] modified the approximate treatment described by Bates to include the dipole velocity formulation and used this treatment to extend the calculations to shorter wavelengths. Their calculations also took into account absorption by the 2s electrons. The theoretical cross sections of Dalgarno and Parkinson are reproduced in Figure 17. In general, the dipole length approximation is preferred at the spectral head, while the velocity approximation is considered more reliable at shorter wavelengths.

More recently, the photoionization cross section of nitrogen atoms has been calculated using the Hartree-Fock approximation for the final states of
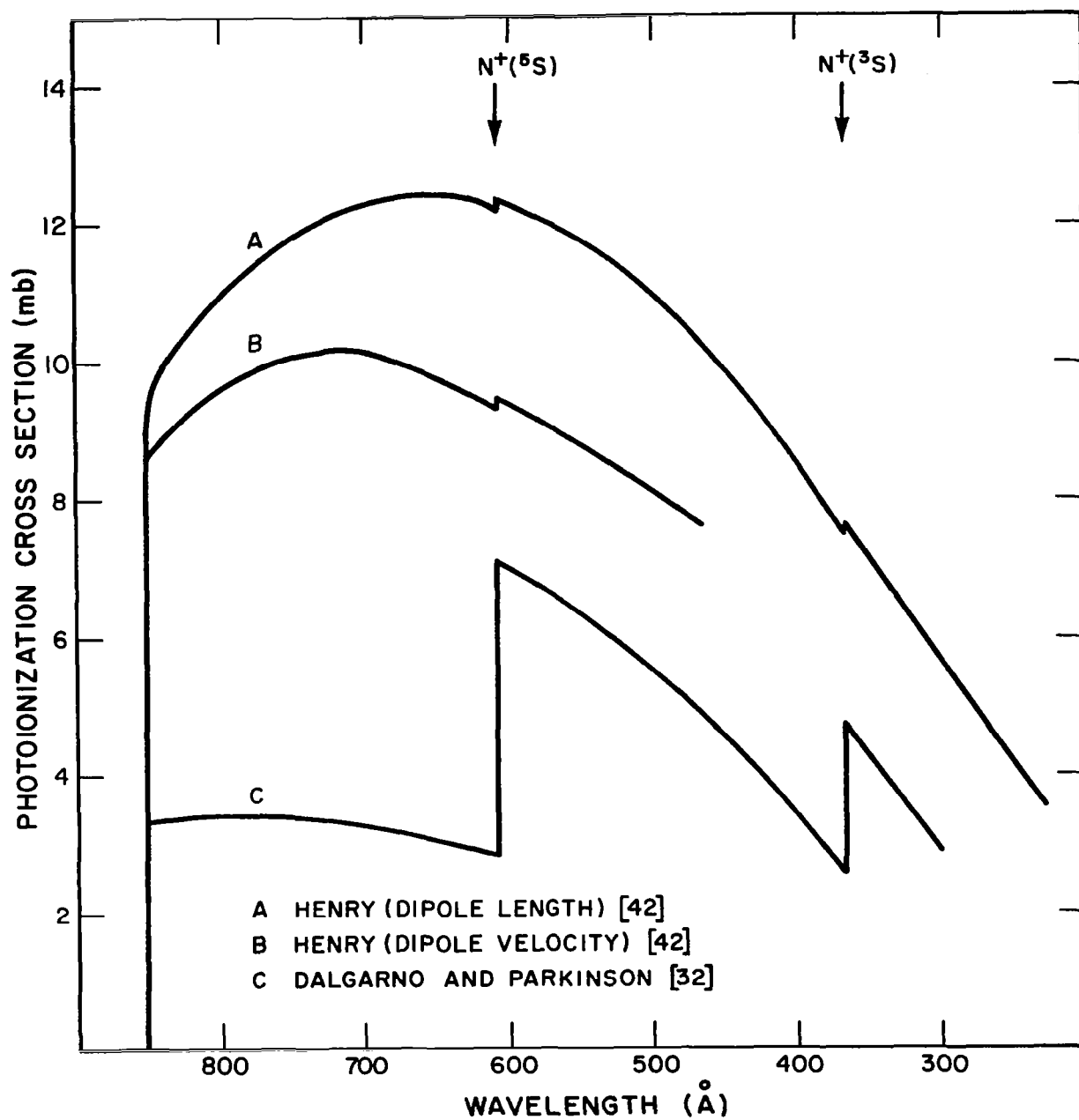
Figure 17. Atomic nitrogen photoionization cross section.

transitions which involve the ejection of an electron from the configuration $1s^2 2s^2 2p^3(^4S)$ [42]; see Figure 17. In the dipole length calculation, the cross section attained a maximum value of 12.4 Mb at 650Å. Both the dipole length and velocity cross sections differed from the results of Dalgarno and Parkinson in that there was only a slight discontinuity at the L_1-absorption edges at 608 and 367Å.

Carroll, et al. [43] have photographed the absorption spectrum of discharged nitrogen and found a new Rydberg series in the region 694 to 612Å. This series was attributed to transitions from the ground $^4S^o$ state of the nitrogen atom to Rydberg terms $2s2p^3(^5S^o)np$: ^4P. All of the absorption lines are broadened owing to autoionization and have the asymmetrical character described by Fano [52] and Fano and Cooper [53]. The wavelengths of these lines are listed in Table 19. The half widths of the absorption part of the lines are also given but are only approximate.

No experimental attempt has been made to obtain the absorption cross section of atomic nitrogen at wavelengths shorter than 400Å. However, a guide to the L_1 absorption cross sections can be obtained by assuming that $\sigma(N) = 1/2 \, \sigma(N_2)$. Experimental values of $1/2 \, \sigma(N_2)$ from 200 to 500Å and from 0.01 to 68Å are listed in Tables 20 and 21, respectively.

New Experiments. — The apparatus used was similar to that described previously in this report (see Figures 2, 10). Undried, tank nitrogen was passed through a microwave discharge and into an absorption cell in which were mounted two fine wire ion collectors. Thus, both the ionization and absorption characteristics of the discharged nitrogen could be examined.

TABLE 19

N I ABSORPTION RYDBERG SERIES[*]

n	$\lambda(\overset{\circ}{A})$	Half-Width cm^{-1}[**]
3	692.70	350
4	647.503	140
5	631.624	78
6	624.059	40
7	619.847	36
8	617.265	26
9	615.627	
10	614.364	21
11	613.500	19
12	612.883	16
13	612.378	
14	611.998	

[*] Carroll, P. K., Huffman, R. E., Larrabee, J. C., and Tanaka, Y.[43]

[**]The half-widths given here, which refer to the absorption part
of the lines, are only approximate. To determine true half-
widths, a full analysis of the Beutler-Fano profiles, which
would require a quantitative study of the relative intensity
distribution in each line, must be made.

TABLE 20

ABSORPTION CROSS SECTIONS OF NITROGEN ASSUMING $\sigma(N) = 1/2\ \sigma(N_2)$[*]

$\lambda(\overset{o}{A})$	$1/2\ \sigma(N_2)_{Mb}$	$\lambda(\overset{o}{A})$	$1/2\ \sigma(N_2)_{Mb}$
209.3	3.2	358.5	7.9
247.2	4.9	362.9	8.1
266.3	5.3	374.4	8.7
283.5	5.5	387.4	9.3
297.6	5.8	428.2	11.0
314.9	6.2	434.3	11.2
323.6	6.6	452.2	11.3
335.1	7.0	463.7	11.3
		508.2	11.4
345.1	7.4	512.1	11.6

[*]Samson, J. A. R. and Cairns, R. B. [17].

102

TABLE 21 (continued)

Shell	$\lambda(\text{Å})$	Experimental [a] $\sigma(N) = 1/2\ \sigma(N_2)$ (Mb)	Semiempirical $\sigma(N)$ (Mb)	
K	3.57	2.23×10^{-3}	----	
	4.36	3.86×10^{-3}	----	
	5.17	6.34×10^{-3}	----	
	6.97	1.50×10^{-2}	----	
	8.32	2.58×10^{-2}	2.44×10^{-2}	Ref. c
	9.87	4.17×10^{-2}	----	
	13.37	8.91×10^{-2}	8.80×10^{-2}	Ref. c
	17.67	1.62×10^{-1}	1.84×10^{-1}	Ref. c
	21.7	----	3.05×10^{-1}	Ref. c
	23.7	----	3.80×10^{-1}	Ref. c
	27.4	----	5.23×10^{-1}	Ref. c
L	31.6	----	3.35×10^{-2}	Ref. c
	36.3	----	4.85×10^{-2}	Ref. c
	44.6	8.88×10^{-2}	8.45×10^{-2}	Ref. c
	68.0	2.53×10^{-1}	----	

[a] Determined from the mass absorption coefficients compiled by Allen, S. J. M. (see Compton, A. H. and Allison, S. K., X-Rays in Theory and Experiment, Van Nostrand, Princeton, N.J., 1935).

[b] Victoreen, J. A., J. Appl. Phys. 20, 1141 (1949).

[c] Henke, B. L., J. Appl. Phys. 28, 98 (1957).

TABLE 21

NITROGEN ABSORPTION CROSS SECTIONS FROM 0.01 to 68Å

Shell	λ(Å)	Experimental [a] $\sigma(N) = 1/2\ \sigma(N_2)$ (Mb)	Semiempirical $\sigma(N)$ (Mb)	
K	0.01	----	1.32×10^{-6}	Ref. b
	0.02	----	1.84×10^{-6}	Ref. b
	0.03	----	2.18×10^{-6}	Ref. b
	0.04	----	2.45×10^{-6}	Ref. b
	0.05	----	2.64×10^{-6}	Ref. b
	0.06	----	2.83×10^{-6}	Ref. b
	0.08	----	3.10×10^{-6}	Ref. b
	0.098	3.32×10^{-6}	----	
	0.100	----	3.32×10^{-6}	Ref. b
	0.200	----	4.20×10^{-6}	Ref. b
	0.710	2.02×10^{-5}	----	
	0.880	3.46×10^{-5}	----	
	1.000	4.90×10^{-5}	5.12×10^{-5}	Ref. b
	1.235	9.18×10^{-5}	----	
	1.389	1.28×10^{-4}	----	
	1.540	1.72×10^{-4}	----	
	1.934	3.25×10^{-4}	----	
	2.50	6.74×10^{-4}	7.2×10^{-4}	Ref. b

Typical results of the absorption experiment are shown in Figure 18(a), (b), and (c) where the intensities of the unattenuated radiation (I_o), the radiation absorbed by ordinary N_2, (I), and the radiation absorbed by discharged N_2, (I′) have been plotted as a function of wavelength. Comparison of the data contained in Figures 18(b) and (c) shows conclusively the presence of species other than ground state molecular and atomic nitrogen. For example, at 880 and 902Å, the ratios I′/I were equal to 0.7 and 0.54, respectively, i.e., there was an increase in absorption at these wavelengths when the gas was discharged. This cannot be attributed to atomic nitrogen but could be caused by vibrationally excited $N_2({}^1\Sigma_g^+)$.

When the gas was discharged, a large constant current was measured to the ion collector wires. By the elimination of other possible mechanisms, the probable source of this current was shown to be excited molecules formed within the discharge. Nitrogen $({}^1\Sigma_g^+)$ molecules excited into vibrational levels for which v is greater than about 15 have sufficient energy to eject electrons upon impact with the collector wires.

The excited molecular species could not be selectively removed, and hence the technique employed could not yield the atom cross section. The findings were consistent with there being copious quantities of vibrationally excited molecules in the discharged gas as was found by Bass [49], Ogawa, et al. [50], and others.
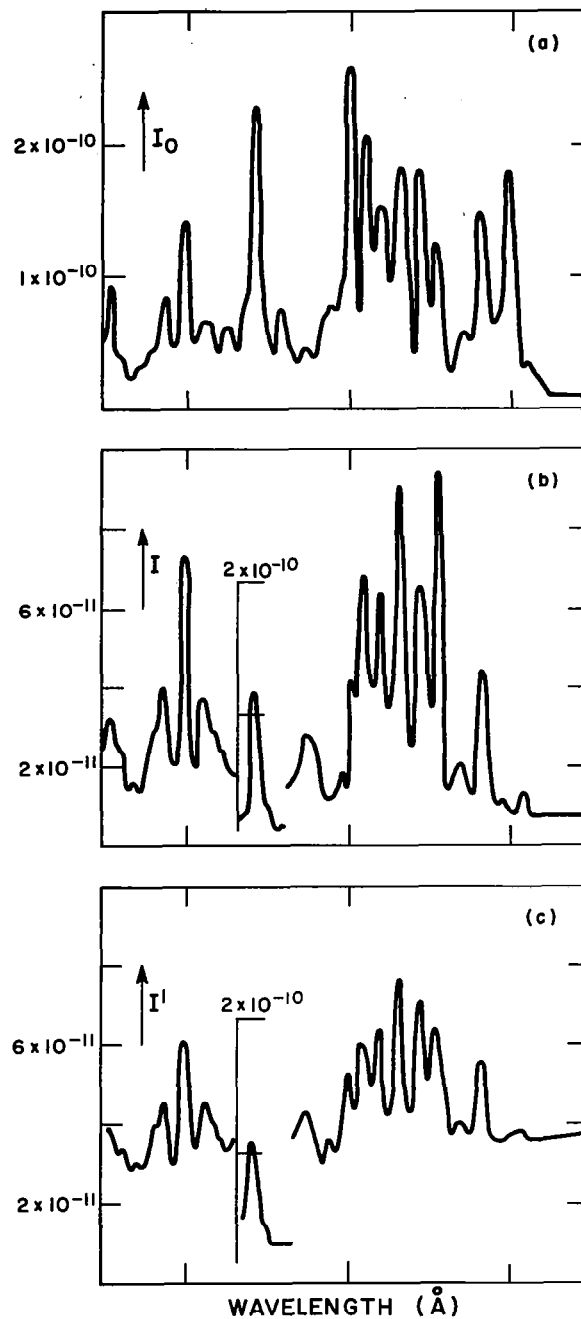
Figure 18. (a) The intensity of light incident upon the absorbing
N₂ as a function of wavelength.
(b) The intensity of light transmitted by normal N₂ as
a function of wavelength.
(c) The intensity of light transmitted by discharged N₂
as a function of wavelength.

CONCLUSION

This report gives an account of the first systematic attempt to measure the photoionization cross sections of atomic H, O, and N. Much quantitative work of considerable interest and difficulty remains to be done as is evidenced by the recent accomplishments of Huffman, et al. [22] and Carroll, et al. [43]. The data which are presently recommended are contained in Figures 19, 20, and 21.

In Figure 19 the theoretical data $\sigma(H)$ contained in Table 1 have been plotted on a scale which allows interpolation between the actual datum points. The experimental work on atomic hydrogen was not free from systematic error but yielded results which were consistent with theory.

The data $\sigma(O)$ are plotted as a function of wavelength in Figure 20. The theoretical curves of Dalgarno, et al. [28] are in fair agreement with experiment but in general indicate a lower cross section. Because of this, the results obtained using the dipole velocity formulation are preferred at wavelengths longer than 732Å. At shorter wavelengths, the dipole length formulation agrees more closely with experiment. The photoionization continuum must be severely distorted, at wavelengths longer than 732Å, by discrete absorption lines many of which are broadened by autoionization [22]. In this spectral region the experimental cross sections must be regarded as the most reliable data. However, it should be remembered; first, that no extrapolation between these datum points is permissible and second, that the details of the experiment were such that the large cross sections, e.g. at 685Å, are probably lower limits to the true values. The Rydberg series converging to the thresholds at
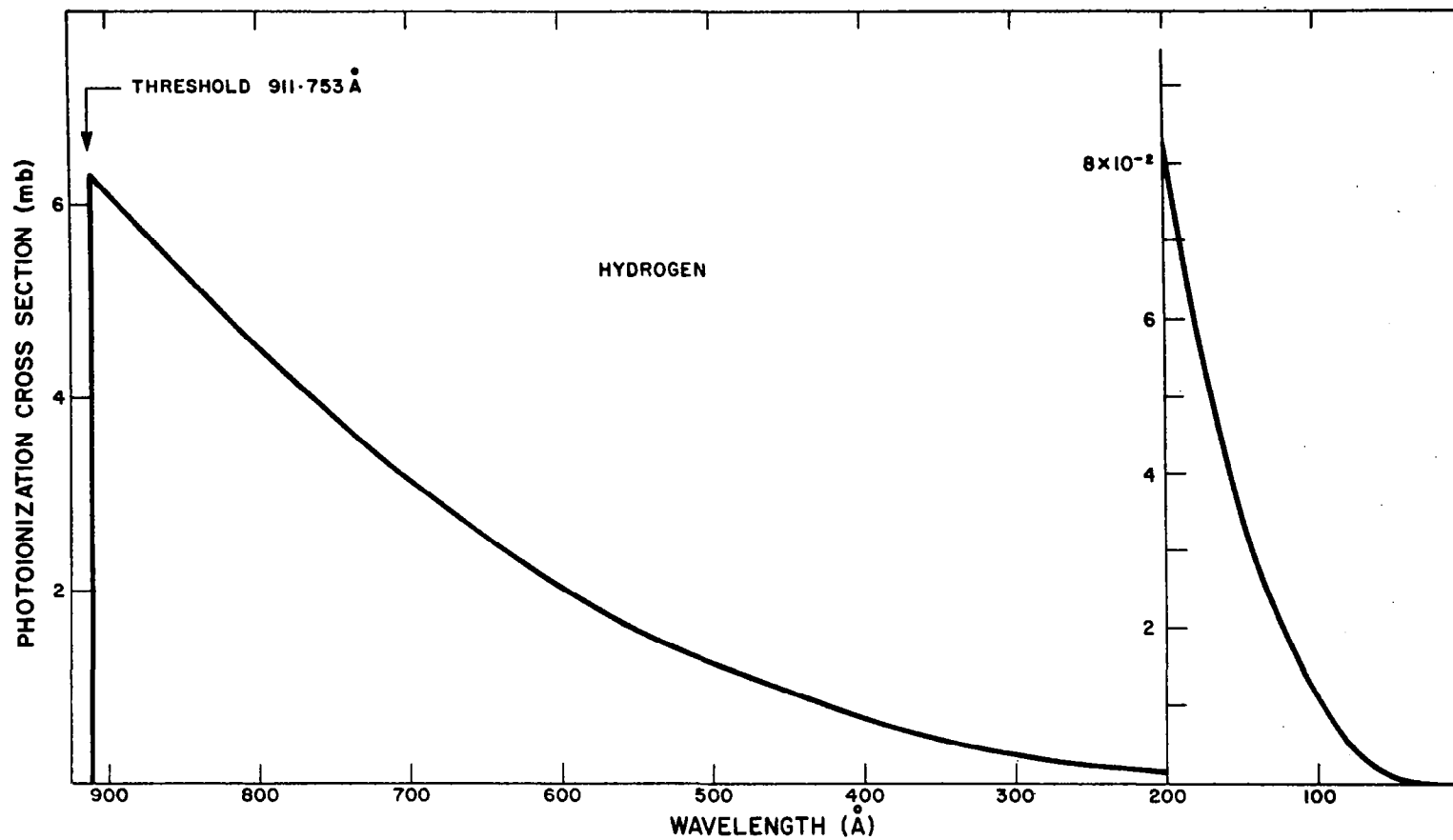
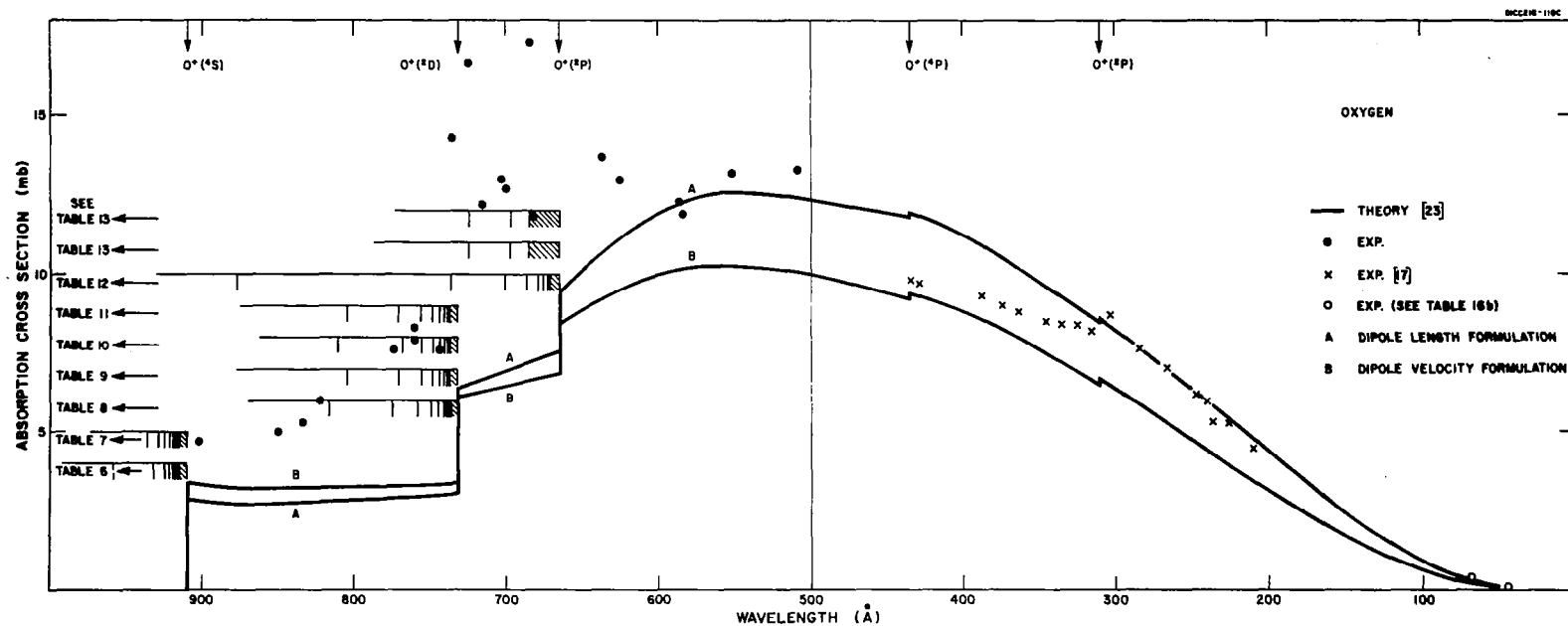Figure 19.   The photoionization cross section of H.

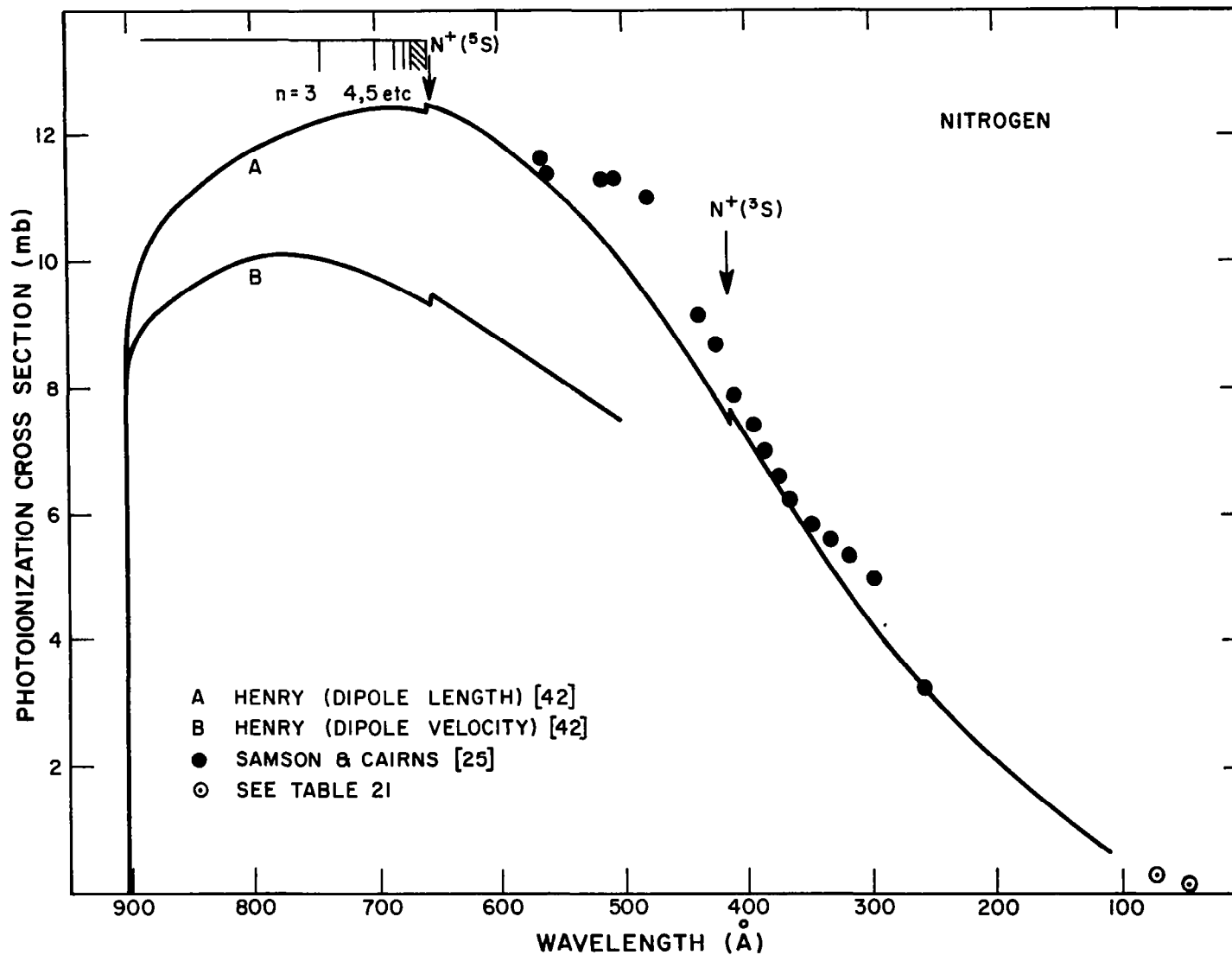Figure 20. The photoionization cross section of O.

Figure 21. The photoionization cross section of N.

732 and 665Å can be expected to disguise and effectively remove the step-like features of the theoretical curve. The preferred data $\sigma(N)$ are shown diagrammatically in Figure 21. The dipole length data of Henry [42] are thought to be more reliable than earlier theories since there is good agreement with the experimental values $1/2 \; \sigma(N_2)$ at wavelengths shorter than 367Å. It should be admitted, however, that this agreement gives no more than a guide to the exactness of any theory. The smoothly varying characteristic of the photoionization cross section will be distorted at the wavelengths listed in Table 19 owing to lines of the Rydberg series converging to 609.76Å. As a result of autoionization, these lines are broadened and asymmetric [43].

References

1. Jennings, K. R. and Linnett, J. W., Nature **182**, 597 (1958).

2. Neynaber, R. H., Marino, L. L., Rothe, E. W., and Trujillo, S. M., Phys. Rev. **124**, 135 (1961).

3. Bak, B. and Rastrup-Andersen, J., Acta Chem. Scand. **16**, 111 (1962).

4. Lichten, W., Phys. Rev. **120**, 848 (1960).

5. Wood, R. W. Proc. Roy. Soc. (London) **97A**, 455 (1920).

6. Bichowsky, F. R. and Copeland, L. C., Nature **120**, 729 (1927).

7. Lord Rayleigh, Proc. Roy. Soc. (London) **91A**, 303 (1915).

8. Rony, P. R., "Studies of Atomic Hydrogen at Low Pressures," AEC Contract No. W-7405-eng-48, UCRL, 1965.

9. Foner, S. N. and Hudson, R. L., J. Chem. Phys. **25**, 601 (1956).

10. Marshall, T. C., Phys. Fluids **5**, 743 (1962).

11. Beynon, J. D. E. and Cairns, R. B., Proc. Phys. Soc. (London) **86**, 1343 (1965).

12. Suguira, Y., J. Phys. Radium **8**, 113 (1927).

13. Gaunt, J. A., Phil. Trans. Roy. Soc. London **A229**, 163 (1930).

14. Menzel, D. H. and Pekeris, C. L., *Monthly Notices Roy. Astron. Soc.* **96**, 77 (1935).

15. Kramers, H. A., Phil. Mag. **46**, 836 (1923).

16. Karzas, W. J. and Latter, R., Astrophys. J. Suppl. Soc. **6**, 167 (1961).

17. Samson, J. A. R. and Cairns, R. B., J. Opt. Soc. Am. **55**, 1035 (1965).

18. Dalgarno, A., GCA Tech. Report No. 62-28-A, 1962.

19. Linnett, J. W. and Marsden, D. G. H., Proc. Roy. Soc. (London) **A234**, 489 (1956).

20. Fite, W. L. and Brackmann, R. T., Phys. Rev. **113**, 815 (1959).

21. Elias, L., Ogryzlo, E. A., and Schiff, H. I., Can. J. Chem. 37, 1608 (1959).

22. Huffman, R. E., Larrabee, J. C., and Tanaka, Y., paper to be published in J. Chem. Phys. (1967).

23. Kaufman, F., Proc. Roy. Soc. (London) A247, 123 (1958).

24. Kaufman, F., J. Chem. Phys. 28, 352 (1958).

25. Samson, J. A. R. and Cairns, R. B., J. Opt. Soc. Am. 56, 769 (1966).

26. Metzger, P. H. and Cook, G. R., J. Quant. Spectrosc. Radiat. Transfer 4, 107 (1964).

27. Samson, J. A. R. and Cairns, R. B., J. Geophys. Res. 69, 4583 (1964).

28. Dalgarno, A., Henry, R. J. W., and Stewart, A. L.,GCA Tech. Rpt. No. 64-1-N (1964).

29. Dalgarno, A. and Lewis, J. T., Proc. Phys. Soc. (London) A69, 285 (1956).

30. Huffman, R. E., Larrabee, J. C., and Tanaka, Y., Phys. Rev. Letters 16, 1033 (1966).

31. Kelley, R. L., "Vacuum Ultraviolet Emission Lines," UCRL Publication 5612.

32. Dalgarno, A. and Parkinson, D., J. Atmospheric Terrest. Phys. 18, 335 (1960).

33. Aboud, A. A., Curtis, J. P., Mercure, R., and Rense, W. A., J. Opt. Soc. Am. 45, 767 (1955).

34. DeReilhac, L. and Damany-Astoin, N., Compt. Rend. 258, 519 (1964).

35. Po Lee, J. Opt. Soc. Am. 45, 703 (1955).

36. Woo, Y. H. and Sun, C. P., Natl. Tsing Hua Univ. Sci. Rept. A4, 398 (1937-1947).

37. Herron, J. and Schiff, H., Can. J. Chem. 36, 1159 (1958).

38. McNeal, R. J. and Cook, G. R., J. Chem. Phys. 45, 3469 (1966).

39. Herzberg, G., Spectra of Diatomic Molecules (D. Van Norstrand Co., New York, 1950), 2nd. ed., p. 560.

40. Ehler, A. W. and Weissler, G. L., J. Opt. Soc. Am. 45, 1035 (1955).

41. Bates, D. R. and Seaton, M. J., Monthly Notices Roy. Astron. Soc. 109, 689 (1949).

42. Henry, R. J. W., J. Chem. Phys. 44, 4357 (1966).

43. Carroll, P. K., Huffman, R. E., Larrabee, J. C., and Tanaka, Y., Astrophysical J. (November 1966).

44. Mitra, S. K., Active Nitrogen - A New Theory (J. N. Bose, Indian Press Ltd., Calcutta, 1945).

45. Oldenberg, O., Planet. & Sp. Sci. 1, 40 (1959).

46. Lichten, W., J. Chem. Phys. 26, 306 (1957).

47. Janin, J., Ann. Phys. (Paris) 1, 548 (1946).

48. Noxon, J. F., Ph.D. Thesis, Harvard University (1957).

49. Bass, A. M., J. Chem. Phys. 40, 695 (1964).

50. Ogawa, M., Tanaka, Y., and Jursa, A. S., J. Chem. Phys. 41, 3351 (1964).

51. Tanaka, Y., Jursa, A. S., LeBlanc, F. J., and Inn, E. C. Y., Planet. & Sp. Sci. 1, 7 (1959).

52. Fano, U., Phys. Rev. 124, 1866 (1961).

53. Fano, U. and Cooper, J. W., Phys. Rev. 137, A1364 (1965).